International Journal of Plasticity 154 (2022) 103309

Contents lists available at ScienceDirect

International Journal of Plasticity

journal homepage: www.elsevier.com/locate/ijplas

A constitutive model for metallic glasses based on two-temperature nonequilibrium thermodynamics

Wei Rao [a,b,c], Yan Chen [a,c,*], Lan-Hong Dai [a,c,*]

[a] State Key Laboratory of Nonlinear Mechanics, Institute of Mechanics, Chinese Academy of Sciences (CAS), Beijing 100190, PR China
[b] Faculty of Materials and Manufacturing, Institute of Mechanics, Beijing University of Technology, Beijing, 100190, PR China
[c] School of Engineering Science, University of Chinese Academy of Sciences, Beijing, 101408, PR China

ARTICLE INFO

Keywords:
Metallic glasses
Constitutive model
Nonequilibrium
Configurational temperature
Deformation mode
Shear band

ABSTRACT

We develop a new finite deformation constitutive model for metallic glass within the framework of irreversible nonequilibrium thermodynamics. To consider the intrinsically out-of-equilibrium characteristics of metallic glass, its total internal energy is divided into two weakly coupled configurational and kinetic subsystems, and configurational temperature coupling with configurational degrees of freedom is introduced as a thermodynamic state variable to characterize the evolution of the disordered structure. Furthermore, the classical shear transformation zone theory is extended by reasonably considering the reverse shear transformation as a form of the relaxation of the strain field, which is stored in the elastic matrix and produced by the constraint of the matrix on shear transformation. With the help of the finite element implementation for the new model, the effectiveness of the proposed model is validated by comparing the modeling stress–strain responses of the macroscopic deformations under different temperatures and strain rates with the experimental results, and the utility of the model for predicting the shear banding behavior of metallic glasses is examined as well. The results therefore show that the constructed constitutive model can not only effectively predict the deformations of metallic glass under different ambient temperatures and applied strain rates, but also reasonably explain the mechanisms of deformation mode evolution and shear band formation.

1. Introduction

The study of the deformation of amorphous solids is a challenging topic with a long history due to the inherent disorder (Nicolas et al., 2018). As an ideal model for the deformation of amorphous and solid-like materials, metallic glasses have attracted considerable attention (Schuh et al., 2007; Falk and Langer, 2011; Rodney et al., 2011; Gao et al., 2011; Wang, 2012; Hufnagel et al., 2016; Jia et al., 2018; Kosiba et al., 2019; Sha et al., 2020; Jiang et al., 2020; Zhang et al., 2022). Different from crystals, it is recognized that the topologically disordered microstructure causes the deformation of metallic glasses to always exhibit an intrinsically out-of-equilibrium phenomenon; in this out-of-equilibrium phenomenon, the internal degrees of freedom in metallic glass are coupled to the applied loading in such a way that the system is persistently driven out of mechanical equilibrium (Bouchbinder and Langer, 2009; Kamrin and Bouchbinder, 2014). Thus, the deformations of metallic glasses always present disparate time and length scales and exhibit diverse

* Corresponding authors at: State Key Laboratory of Nonlinear Mechanics, Institute of Mechanics, Chinese Academy of Sciences (CAS), Beijing 100190, PR China.
E-mail addresses: chenyan@lnm.imech.ac.cn (Y. Chen), lhdai@lnm.imech.ac.cn (L.-H. Dai).

https://doi.org/10.1016/j.ijplas.2022.103309
Received 22 February 2022; Received in revised form 12 April 2022;
Available online 15 April 2022

modes with changes in the loading conditions (Karmakar et al., 2014; Schuh et al., 2007). At elevated temperatures, they display a liquid-like behavior that follows Newtonian or non-Newtonian flow laws when subjected to deformation (Spapaen 1977; Wang et al., 2014). When the ambient temperature is close to or greater than the glass transition temperature they deform homogeneously, and their elongation can reach 1000% under quasi-static loading (Kawamura et al., 1998). Even at a high strain rate their elongation can also reach as high as 20%, but if the loading rate is large enough, metallic glasses exhibit nonhomogeneous behavior where shear localization occurs before failure. However, at room temperature, almost all of their inelastic deformations are always localized into shear bands with nanoscale thicknesses (Dai and Bai, 2007; Greer et al., 2013; Jiang et al., 2021). Such significant shear localization would ultimately result in their very limited ductility at room temperature (Sun and Wang, 2015; Tandaiya et al., 2009).

Interestingly, these diverse deformation modes of metallic glasses are underlain by the same fundamental flow event known as the shear transformation zone (STZ), which emanated from the flow defect theory of Turnbull and Cohen (1970), Spaepen (1977), Argon (1979), and Falk and Langer (1998), where localized clusters of molecules undergo irreversible rearrangements with the help of the applied shear stress and thermal fluctuations. In a very rough sense, the STZ in amorphous materials plays the role of dislocations in crystals by acting as agents of plastic deformation. In fact, some results have shown that the different modes of deformation are then expected to be comprised of either the uncorrelated activation of STZs uniformly distributed throughout the sample, as in the case of homogeneous deformation, or highly correlated activation of STZs in a localized band, as in the case of inhomogeneous deformation (Homer et al., 2010). Nevertheless, it has been realized that the classical shear transformation does not consider the effect of shear transformation on the surrounding elastic matrix. In fact, the constraint of the elastic matrix on shear transformation can result in a strain energy stored in this matrix once the shear transformation occurs, and this stored energy can be regarded as the driving force of the inverse shear transformation. Therefore, how to consider the constraint of the surrounding elastic matrix on the subsequent shear transformation is a critical issue for the shear transformation model.

As is known, small-scale dynamics are highly heterogeneous, intermittent and seemingly nondeterministic, while the emergent macroscopic phenomena are quite robust. Thus, how to effectively bridge over widely separate scales is crucial for research on the deformations of metallic glasses. In view of the success of equilibrium statistical thermodynamics in bridging over widely separated scales, an effective disorder temperature theory has been proposed for nonequilibrium deformation behaviors of amorphous materials in the past few decades by drawing from the statistical concepts and the most general form of the laws of thermodynamics (Bouchbinder and Langer, 2009; Cugliandolo, 2011; Xue et al., 2017). To date, the effective disorder temperature is emerging as an essential ingredient in theories of nonequilibrium phenomena in amorphous materials. The effectiveness of its application to the nonequilibrium behavior of amorphous polymers (Xiao et al, 2013; Xiao and Nguyen, 2015) and soft glassy rheology (Sollich and Cates, 2012) has been widely confirmed. Recently, some studies have introduced the effective disorder temperature into the STZ theory of large-scale plastic deformation in metallic glasses (Bouchbinder, et al., 2007; Manning et al., 2009), and the nature of shear-banding instabilities has been reasonably explained. As with the flow-defect picture, the effective disorder temperature idea also originated from Cohen and Turnbull's theory of glasses (Cohen and Turnbull, 1959). Other investigators, notably Spaepen (1977), described the intrinsically disordered state of amorphous materials by introducing the free volume. Those authors perceptively recognized that the relevant definition of free volume is not as an extensive quantity—the extensive excess volume measured from some densely packed state, but as an intensive one—the inverse of the derivative of a configurational entropy with respect to the volume (Shi, et al., 2007). Many scholars currently believe that it is more effective to conduct a thermodynamic analysis in terms of energy rather than volume, since the mechanical behavior of metallic glass is determined by the interactions among their elementary ingredients, and the introduction of effective disorder temperature theory would lead us to new discoveries in the nonequilibrium deformation of metallic glasses (Falk and Langer, 2011).

Modeling the nonequilibrium deformation behaviors of metallic glasses can help us better understand their deformation nature. Thus, many worthy models of the deformation of metallic glass have been performed (Tandaiya et al., 2008; Rondey et al., 2011; Takeuchi and Edagawa, 2011; Singh et al., 2013, 2014; Kondori, et al., 2018; Liu et al., 2020; Dutta and Narasimhan, 2020; Rodney et al., 2009; Thamburaja and Liu, 2014; Kondori et al., 2016; Rao et al., 2019; Gan et al., 2019; Vasoya et al., 2020; Xie et al., 2019; Lin et al., 2020; Van Loock et al., 2021; Yuan et al., 2020). Among them, the constitutive models play a vitally important role since they can provide an effective prediction for the deformation of metallic glass at engineering scales. For this reason, many constitutive models, such as the models established by Huang and Suo (2002), Anand and Su (2005 and 2007), Henann and Anand (2008), Thamburaja and Ekambaram (2007), Yang et al. (2006), Rao et al. (2018), Zhu et al. (2021), have been developed in the past decades based on the free volume theory of Spaepen (1977). With the help of these constitutive models, many key points in the deformation of metallic glass, such as the evolution of the shear band (Yang et al., 2006), origin of shear banding instability (Jiang and Dai, 2009), length scale effects (Bargmann et al., 2014; Thamburaja et al., 2011), shear-induced dilatation (Zhu et al., 2021), failure mechanisms (Anand and Su, 2005; Tandaiya et al., 2009. Dutta et al., 2018; Rao et al., 2018; Tang et al., 2021), rheological behavior (Cheng et al., 2021), have been deeply investigated, and some important conclusions have deepened the understanding of amorphous deformations. However, since the nonequilibrium characteristics in metallic glasses are difficult to capture by introducing the free volume as a state variable, the adopted continuum models are often changed to accommodate the different modes of deformation during modeling deformations of metallic glass under different loading conditions (Homer et al., 2016). Recently, along with the effective temperature introduced into STZ theories, Kamrin and Bouchbinder (2014) developed a two-temperature continuum thermodynamics theory for deforming amorphous solids. In their theory, the key idea is that the degree of the system is decomposed into two weakly interacting subsystems, i.e., a fast kinetic one that can reach an equilibrium state instantaneously and a slow configurational subsystem that is permanent in a quasi-equilibrium state. Such a framework provides an effective and distinct idea for developing a constitutive model for the nonequilibrium deformation of metallic glasses.

In this work, referring to the two-temperature continuum thermodynamics theory and STZ theory, a three-dimensional finite

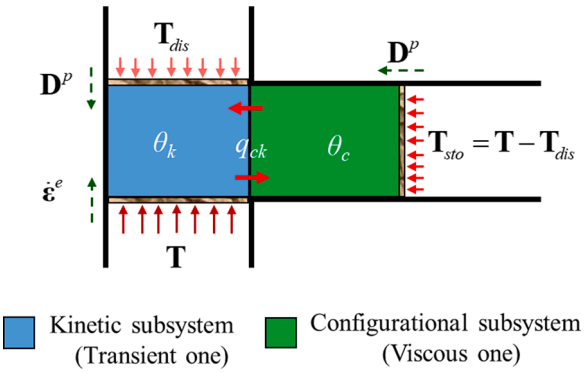

Fig. 1. Diagram for the modeling procedure. In this diagram, the stresses ($\mathbf{T}$, $\mathbf{T}_{dis}$ and $\mathbf{T}_{sto}$) are regarded as pressures on the piston, the strain rate and stretching one ($\dot{\varepsilon}^e$ and $\mathbf{D}^p$) are regarded as the piston speeds. θ_k and θ_c are the temperatures characterizing degrees of freedom of kinetic and configurational subsystems, respectively. q_{ck} is the exchange energy between the kinetic and configurational subsystems, which drives the two subsystems towards equilibrium.

deformation constitutive model is developed within the new framework of irreversible nonequilibrium thermodynamics so that the nonequilibrium deformation of metallic glasses can be explained from an essential perspective. In this new framework, the system is decomposed into sub-balanced kinetic and quasi-equilibrium configurational subsystems in the reference configuration so that the kinetic and configurational processes are characterized by their own thermodynamic quantities, where the sum of the kinetic and configurational processes determines the properties of the entire system. Furthermore, the energy exchange between the two subsystems is introduced to drive the subsystems toward equilibrium. To capture the inelastic deformation mechanisms of metallic glass, an energy field, which is stored in the surrounding elastic matrix, is introduced into the classical shear transformation zone theory. The production of such an energy field is related to the constraint of the matrix on shear transformation, and its relaxation is in the form of an inverse shear transformation. Finally, based on the finite element implementation of the new constitutive model, both the macroscopic compressive deformations under different strain rates and ambient temperatures are predicted by using the finite element methods, as well as the shear localization during room-temperature quasi-static deformations. The consistency of the predicted results with the experimental and theoretical results demonstrates the reasonability and validity of the proposed model.

2. Constitutive model

The nonequilibrium deformation of metallic glass, which is mediated by localized shear-driven rearrangements involving a small number of basic elements, is a complex elasto-viscoplastic process. In the process of deformation, the time scale of structural relaxation is much slower than the fast timescale characterizing random thermal vibrations around a mechanically stable microscopic configuration, which leads to the degree of freedom of configurational subsystem undergoing structural relaxation falling out of an internal equilibrium with that of kinetic subsystem undergoing random thermal vibrations. To reasonably capture the intrinsically nonequilibrium characteristic of metallic glasses, a new framework of irreversible continuum nonequilibrium thermodynamics is provided by referring to the work of Kamrin and Bouchbinder (2014). Then, based on an extended STZ theory, a new constitutive model for metallic glass is constructed using such a framework. The modeling diagram is shown in Fig. 1.

From Fig. 1, the nonequilibrium system of metallic glasses is completely decoupled into two separate subsystems. Energy exchange exists between these two subsystems and drives the nonequilibrium system of metallic glasses to gradually approach an equilibrium state. In the kinetic subsystem, the microscopic events are considered atomic short-distance motion around a mechanically stable microscopic configuration, and their timescale is so small that their mechanical responses can be regarded as immediate events. Thus, an affine deformation is deemed the event of the kinetic subsystem. Instead, the occurrence of microevents in the configurational subsystem is regarded as the instability of the atom cluster; thus, the timescale of the configurational subsystem is always much slower than that of the kinetic subsystem. Furthermore, as the rearrangement of microstructure occurs, we should account for the fluctuations in energy in different subsystems. During nonaffine deformation, the nonequilibrium nature of metallic glasses is characterized by the energy distribution of two subsystems. Generally, the distribution of energy into two subsystems cannot make the total entropy of the system reach the maximum value, as discussed in the work of Kamrin and Bouchbinder (2014). In this work, the energy allocated to the kinetic and configurational subsystems is described by $\mathbf{T}_{dis} : \mathbf{D}^p$ and $\mathbf{T}_{sto} : \mathbf{D}^p$ during the nonaffine deformation, where the exchange energy of q_{ck} between two subsystems always drives the total entropy to the maximum value.

2.1. Kinematics

Considering a deformable body identified with the region B and assuming that $\mathbf{X}$ is an arbitrary position vector of a certain material point in the fixed reference configuration where $\mathbf{x} = \mathbf{x}(\mathbf{X}, t)$ is the corresponding space position vector denoted at the current time, the deformation gradient $\mathbf{F}$, velocity $\mathbf{v}$ and velocity gradient $\mathbf{L}$ can be written as

$$\mathbf{F}=\frac{\partial \mathbf{x}}{\partial \mathbf{X}},\quad \mathbf{v}=\dot{\mathbf{x}},\qquad \mathbf{L}=\mathrm{grad}(\mathbf{v})=\dot{\mathbf{F}}\mathbf{F}^{-1} \tag{1}$$

Hereafter, the variable $\dot{\mathbf{A}}$ denotes the material time derivative of A, which is an arbitrary scalar or tensor field.

In the classical finite deformation framework, the elastic deformation and inelastic deformation are coupled with one another. Thus, adopting the Kroner-Lee decomposition, the deformation gradient $\mathbf{F}$ can be given as

$$\mathbf{F}=\mathbf{F}^{e}\mathbf{F}^{p} \tag{2}$$

where the tensors $\mathbf{F}^{e}$ and $\mathbf{F}^{p}$ denote the elastic distortion and inelastic distortion, respectively.

To eliminate the rigid rotation part, the elastic deformation gradient can be divided into two parts:

$$\mathbf{F}^{e}=\mathbf{R}^{e}\mathbf{U}^{e},\quad \mathbf{R}^{e\mathrm{T}}=\mathbf{R}^{e-1},\quad \mathbf{C}^{e}=\mathbf{U}^{e2}=\mathbf{F}^{e\mathrm{T}}\mathbf{F}^{e} \tag{3}$$

where the orthogonal tensor $\mathbf{R}^{e}$ is an elastic rotation tensor that characterizes the rigid rotation and the symmetric positive definite tensors $\mathbf{U}^{e}$ and $\mathbf{C}^{e}$ are the right elastic stretch tensor and right elastic Cauchy-Green tensor, respectively, which characterize the elastic deformation.

From Eqs. (1) and (2), it can be determined that

$$\mathbf{L}=\mathbf{L}^{e}+\mathbf{F}^{e}\mathbf{L}^{p}\mathbf{F}^{e-1} \tag{4}$$

where $\mathbf{L}^{e}=\dot{\mathbf{F}}^{e}\mathbf{F}^{e-1}$ and $\mathbf{L}^{p}=\dot{\mathbf{F}}^{p}\mathbf{F}^{p-1}$ are the elastic and inelastic velocity gradient tensors, respectively.

Using additive decomposition, the elastic and inelastic velocity gradient tensors can be divided as

$$\mathbf{D}^{e}=\frac{1}{2}\left(\mathbf{L}^{e}+\mathbf{L}^{e\mathrm{T}}\right),\quad \mathbf{W}^{e}=\frac{1}{2}\left(\mathbf{L}^{e}-\mathbf{L}^{e\mathrm{T}}\right) \tag{5a}$$

$$\mathbf{D}^{p}=\frac{1}{2}\left(\mathbf{L}^{p}+\mathbf{L}^{p\mathrm{T}}\right),\quad \mathbf{W}^{p}=\frac{1}{2}\left(\mathbf{L}^{p}-\mathbf{L}^{p\mathrm{T}}\right) \tag{5b}$$

where the symmetric tensors $\mathbf{D}^{e}$ and $\mathbf{D}^{p}$ represent the elastic and inelastic stretching tensors, respectively, and the skew-symmetric tensors $\mathbf{W}^{e}$ and $\mathbf{W}^{p}$ denote the elastic and inelastic spin tensors, respectively.

Following the work of Anand and Gurtin (2003), inelastic flow can be treated as irrational; thus,

$$\mathbf{W}^{p}=\mathbf{0}\quad\Rightarrow\quad \mathbf{D}^{p}=\mathbf{L}^{p} \tag{6}$$

From the work of Rao et al. (2018), we can define an elastic logarithmic strain tensor $\mathbf{E}^{e}$ in the reference configuration as

$$\mathbf{E}^{e}=\frac{1}{2}\ln\mathbf{C}^{e}=\ln\mathbf{U}^{e} \tag{7}$$

2.2. Thermodynamic balance

According to the work of Thamburaja and Ekambaram (2007), the momentum conservation in the reference configuration P_0 can be written as

$$\int_{\partial P_0}\mathbf{S}\mathbf{n}_0\mathrm{d}S_0+\int_{P_0}\mathbf{b}\mathrm{d}V_0=\frac{\mathrm{d}}{\mathrm{d}t}\int_{P_0}\rho_0\mathbf{v}\mathrm{d}V_0 \tag{8}$$

Here, $\mathrm{d}S_0$ and $\mathrm{d}V_0$ are the area and volume integrals in the reference configuration, respectively, $\mathbf{n}_0$ is the unit vector along the face normal, $\mathbf{S}=J\mathbf{T}\mathbf{F}^{-\mathrm{T}}$ is the first Piola–Kirchoff stress, $\mathbf{T}$ is the Cauchy stress, $J=\det(\mathbf{F})$ is the volume Jacobian, $\mathbf{b}$ denotes the macroscopic body force in the reference volume determinant, and ρ_0 is the referential mass density.

As is known, Eq. (8) is always tenable for any size and shape of the reference configuration P_0. By using Gauss's law, it yields

$$\mathrm{Div}\mathbf{S}+\mathbf{b}-\rho_0\mathbf{v}=\mathbf{0} \tag{9}$$

Based on the work of Thamburaja and Ekambaram (2007), the first law of thermodynamics in the reference configuration P_0 can be given as

$$\dot{\int_{P_0}\varepsilon dV_0}=\int_{\partial P_0}\left(\mathbf{S}^{T}\mathbf{v}-\mathbf{q}\right)\mathbf{n}_0 dS_0+\int_{P_0}(\mathbf{b}\cdot\mathbf{v}+q)dV_0 \tag{10}$$

where ε is the internal energy per unit reference volume, where $\mathbf{q}$ and q denote the referential heat flux vector and the heat supply rate per unit reference volume, respectively.

Combining Eqs. (9) and (10), it can be determined that

$$\dot{\varepsilon}=\mathbf{S}\cdot\dot{\mathbf{F}}-\mathrm{Div}(\mathbf{q})+q \tag{11}$$

Similarly, the second law of thermodynamics in the reference configuration P_0 can be given as

$$\overline{\int_{P_0} \eta dV_0} \geq \int_{\partial P_0} \mathbf{j}\mathbf{n}_0 dS_0 + \int_{P_0} j dV_0 \tag{12}$$

where η is the entropy per unit reference volume, and $\mathbf{j}$ and j denote the referential entropy flux vector and entropy supply rate per unit reference volume, respectively.

Using the divergence theorem, a local form of entropy inequality can be obtained from Eq. (12), namely,

$$\dot{\eta} \geq -\mathrm{Div}\mathbf{j} + j \tag{13}$$

According to the assumption of Kamrin and Bouchbinder (2013), the state of each system can be characterized by its own thermodynamic quantities, and the state of the nonequilibrium system is equivalent to an additive combination of the kinetic/vibrational and configurational contributions, as shown in Fig. 1. Thus,

$$\varepsilon = \varepsilon_k + \varepsilon_c, \quad \eta = \eta_k + \eta_c \tag{14a}$$

$$\mathbf{q} = \mathbf{q}_k + \mathbf{q}_c, \quad \mathbf{j} = \mathbf{j}_k + \mathbf{j}_c \tag{14b}$$

where ε_k and ε_c are the kinetic and configurational internal energies per unit reference volume, respectively, η_k and η_c are the kinetic and configurational entropy per unit reference volume, respectively, $\mathbf{q}_k$ and $\mathbf{j}_k$ are the kinetic heat and entropy fluxes that result from the passage of random vibrational motion into (out of) a part, and $\mathbf{q}_c$ and $\mathbf{j}_c$ are the configurational heat and entropy fluxes that result from disturbing the neighboring structural assembly in a random fashion during rearrangements of the structure. Hereafter, the subscripts k and c denote the quantity belonging to kinetic/vibrational and configurational systems, respectively.

According to the physical essence of the configurational subsystem, it is not difficult to assume that the configurational internal energy is a non-source field. Thus,

$$q = q_k, \quad j = j_k \tag{15}$$

where q_k and j_k are the kinetic heat and entropy supply rates per unit reference volume, respectively.

Based on the classical Clausius-Duhem inequality, the temperature field θ bridges $\mathbf{q}$ (q) and $\mathbf{j}$ (j) by $\mathbf{j} = \frac{\mathbf{q}}{\theta}$ ($j = \frac{q}{\theta}$). By analogy, some similar function relations can be given as

$$\mathbf{j}_k = \frac{\mathbf{q}_k}{\theta_k}, \quad \mathbf{j}_c = \frac{\mathbf{q}_c}{\theta_c} \tag{16a}$$

$$j_k = \frac{q_k}{\theta_k} \tag{16b}$$

where θ_k and θ_c denote the kinetic and configurational temperatures, respectively, which describe the degrees of freedom of the atomic vibrations and configuration. As is known, the degree of freedom of atomic vibrations manifests as the part of the internal energy that arises due to the particles rattling about some mean positions within their cages of nearest neighbors. In general, it rapidly equilibrates with an external bath. Instead, the configurational subsystem achieves equilibrium through the coordinated rearrangement of atom clusters, and it has a much larger time scale than atom vibrations. Thus, the out-of-equilibrium system is always satisfied with $\theta_c \neq \theta_k$, whereas $\theta_c = \theta_k$ indicates internal equilibrium.

From Eqs. (11), (13) and (14a, b), the local form of the first and second law of thermodynamics in the reference configuration can be rewritten as

$$\dot{\varepsilon} = \mathbf{S} \cdot \dot{\mathbf{F}} - \mathrm{Div}(\mathbf{q}_k) - \mathrm{Div}(\mathbf{q}_c) + q_k \tag{17a}$$

$$\dot{\eta} \geq -\mathrm{Div}\left(\frac{\mathbf{q}_k}{\theta_k}\right) - \mathrm{Div}\left(\frac{\mathbf{q}_c}{\theta_c}\right) + \frac{q_k}{\theta_k} \tag{17b}$$

Substituting Eqs. (2)–(4) into Eq. (17a), it can be determined that

$$\dot{\varepsilon} = \mathbf{T}^* : \dot{\mathbf{H}}^e + \overline{\mathbf{T}} : \mathbf{D}^p - \mathrm{Div}(\mathbf{q}_k) - \mathrm{Div}(\mathbf{q}_c) + q_k \tag{18a}$$

with

$$\mathbf{T}^* = J\mathbf{R}^{eT}\mathbf{T}\mathbf{R}^e \tag{18b}$$

$$\overline{\mathbf{T}} = \mathbf{U}^e\mathbf{T}^*\mathbf{U}^{e-1} \tag{18c}$$

$$\dot{\mathbf{H}}^e = \mathrm{sym}\left(\dot{\mathbf{U}}^e \cdot \mathbf{U}^{e-1}\right) \tag{18d}$$

It should be noted that $\mathbf{T}^*$ and $\overline{\mathbf{T}}$ are the frame-invariant stress tensors.

Following the work of Kamrin and Bouchbinder (2014), the total internal energy of the system is equal to the sum of the internal energies of the two subsystems. As is known, the elastic response has the same time scale as the atomic vibration; thus, we classify it into the kinetic internal energy. In addition, some studies have shown that both the evolution of the structure disorder degree and a temperature rise may occur along with inelastic deformation, which indicates that inelastic work affects both subsystems. The inelastic work belonging to the kinetic subsystem would be converted into thermal energy and then dissipate; thus, we call this part of inelastic work the inelastic dissipation work. Instead, the inelastic work related to the configurational subsystem would change the configuration and be stored in the system; thus, we call this part the storage energy. Moreover, it should be noted that there is a slow energy exchange between the two subsystems so that the total entropy can be maximized. Thus, we can give the energy balance for these two subsystems as

$$\dot{\varepsilon}_k = \mathbf{T}^* : \mathbf{H}^e + \overline{\mathbf{T}}_{dis} : \mathbf{D}^p - \mathrm{Div}(\mathbf{q}_k) + q_k + q_{ck} \tag{19a}$$

$$\dot{\varepsilon}_c = \overline{\mathbf{T}}_{sto} : \mathbf{D}^p - \mathrm{Div}(\mathbf{q}_c) - q_{ck} \tag{19b}$$

where q_{ck} is the scalar internal heat flow, which is used to describe the energy exchange between two subsystems, and $\overline{\mathbf{T}}_{dis}$ and $\overline{\mathbf{T}}_{sto}$ are the dissipation stress and storage one, respectively, which satisfy $\overline{\mathbf{T}} = \overline{\mathbf{T}}_{dis} + \overline{\mathbf{T}}_{sto}$.

Substituting Eqs. (14a, b), (15), (16a, b) and (19a, b) into Eq. (17b), the entropy inequality can be rewritten as

$$\begin{aligned} &\dot{\eta}_k + \dot{\eta}_c + \frac{1}{\theta_k}\left(\mathbf{T}^* : \mathbf{H}^e + \overline{\mathbf{T}}_{dis} : \mathbf{D}^p - \dot{\varepsilon}_k + q_{ck} - \frac{\mathbf{q}_k}{\theta_k}\cdot\nabla\theta_k\right) \\ &+\frac{1}{\theta_c}\left(\overline{\mathbf{T}}_{sto} : \mathbf{D}^p - \dot{\varepsilon}_c - q_{ck} - \frac{\mathbf{q}_c}{\theta_c}\cdot\nabla\theta_c\right) \geq 0 \end{aligned} \tag{20}$$

According to the work of Kamrin and Bouchbinder (2014), the kinetic and configurational Helmholtz free energy per unit reference volume can be respectively defined as

$$\psi_k = \varepsilon_k - \eta_k\theta_k \Rightarrow \dot{\psi}_k = \dot{\varepsilon}_k - \dot{\eta}_k\theta_k - \eta_k\dot{\theta}_k \tag{21a}$$

$$\psi_c = \varepsilon_c - \eta_c\theta_c \Rightarrow \dot{\psi}_c = \dot{\varepsilon}_c - \dot{\eta}_c\theta_c - \eta_c\dot{\theta}_c \tag{21b}$$

where ψ_k and ψ_c are the kinetic and configurational Helmholtz free energy per unit reference volume, respectively.

Substituting Eq. (21a, b) into Eq. (20) yields

$$\begin{aligned} &\frac{1}{\theta_k}\left(\mathbf{T}^* : \mathbf{H}^e + \overline{\mathbf{T}}_{dis} : \mathbf{D}^p - \dot{\psi}_k - \eta_k\dot{\theta}_k + q_{ck} - \frac{\mathbf{q}_k}{\theta_k}\cdot\nabla\theta_k\right) \\ &+\frac{1}{\theta_c}\left(\overline{\mathbf{T}}_{sto} : \mathbf{D}^p - \dot{\psi}_c - \eta_c\dot{\theta}_c - q_{ck} - \frac{\mathbf{q}_c}{\theta_c}\cdot\nabla\theta_c\right) \geq 0 \end{aligned} \tag{22}$$

2.3. Free energy

Internal variables carry information on the microstructure state and determine the following inelastic responses. The thermodynamic state of the material can be fully defined by certain state variables. In amorphous solids, its deformation includes both the equilibrium phenomenon and the quasi-equilibrium phenomenon. The equilibrium phenomenon is a type of immediate response. We assume that the equilibrium phenomenon can be characterized by the kinetic temperature θ_k and the elastic deformation $\mathbf{C}^e$, while the quasi-equilibrium phenomenon is hysteretic and can be captured by the configurational temperature θ_c and the inelastic shear strain γ. It should be noted that the shear inelastic strain is contributed by two parts: the one is along with the shear transformation, similar to the accumulated plastic strain of plasticity theory; the other one is caused by the reverse shear transformation which is the mechanism of a special structural relaxation. Most notably, since the time-scale of such structural relaxation is small, the deformation dominated by reverse shear transformation is easy to be regarded as the viscoelastic deformation at the macro-scale. Then the functional forms of the kinetic and configurational Helmholtz free energy per unit reference volume are assumed as

$$\psi_k = \widehat{\psi}_k(\mathbf{C}^e, \theta_k) \tag{23a}$$

$$\psi_c = \widehat{\psi}_c(\theta_c, \gamma) \tag{23b}$$

From the principle of material frame invariance, ψ_k and ψ_c are the frame-invariance functions, since $\mathbf{C}^e$, θ_k, θ_c and γ are the frame-invariance variables.

The time derivatives of ψ_k and ψ_c are then taken as

$$\dot{\psi}_k = \frac{\partial\psi_k}{\partial\mathbf{C}^e} : \dot{\mathbf{C}}^e + \frac{\partial\psi_k}{\partial\theta_k}\dot{\theta}_k \tag{24a}$$

$$\dot{\psi}_c = \frac{\partial \psi_c}{\partial \theta_c}\dot{\theta}_c + \frac{\partial \psi_c}{\partial \gamma}\dot{\gamma} \tag{24b}$$

Substituting Eq. (24a, b) into Eq. (22), it yields

$$-\frac{1}{\theta_k}\left(\frac{\partial \psi_k}{\partial \theta_k}+\eta_k\right)\dot{\theta}_k + \frac{1}{\theta_k}\left(\mathbf{T}^* - 2\mathbf{U}^e\frac{\partial \psi_c}{\partial \mathbf{C}^e}\mathbf{U}^e\right) : \dot{\mathbf{H}}^e - \frac{1}{\theta_c}\left(\frac{\partial \psi_c}{\partial \theta_c}+\eta_c\right)\dot{\theta}_c + \Pi \geq 0 \tag{25}$$

where

$$\Pi = \frac{1}{\theta_k}\left(\overline{\mathbf{T}}_{dis} : \mathbf{D}^p + q_{ck} - \frac{\mathbf{q}_k}{\theta_k}\cdot\nabla\theta_k\right) + \frac{1}{\theta_c}\left(\overline{\mathbf{T}}_{sto} : \mathbf{D}^p - q_{ck} - \frac{\mathbf{q}_c}{\theta_c}\cdot\nabla\theta_c - \frac{\partial \psi_c}{\partial \gamma}\dot{\gamma}\right) \tag{26}$$

is the total dissipation per unit reference volume.

Eq. (11) should always be satisfied with arbitrary values of the elastic strain rate tensor $\dot{\mathbf{H}}^e$, $\dot{\theta}_k$ and $\dot{\theta}_c$, yielding

$$\mathbf{T}^* = 2\mathbf{U}^e\frac{\partial \psi_c}{\partial \mathbf{C}^e}\mathbf{U}^e \tag{27a}$$

$$\eta_k = -\frac{\partial \psi_k}{\partial \theta_k} \tag{27b}$$

$$\eta_c = -\frac{\partial \psi_c}{\partial \theta_c} \tag{27c}$$

2.4. Dissipation inequality

Along with Eq. (27a, b, c), the local dissipation inequality can be rewritten in the reference configuration as

$$\Pi = \underbrace{\left(\frac{\overline{\mathbf{T}}_{dis}}{\theta_k}+\frac{\overline{\mathbf{T}}_{sto}}{\theta_c}\right) : \mathbf{D}^p - \frac{1}{\theta_c}\frac{\partial \psi_c}{\partial \gamma}\dot{\gamma}}_{\text{Inelasticdissipation}} + \underbrace{q_{ck}\left(\frac{1}{\theta_k}-\frac{1}{\theta_c}\right)}_{\text{Disspationduetodistributionofenergyintwosubsystem}} - \underbrace{\frac{\mathbf{q}_k}{\theta_k^2}\cdot\nabla\theta_k}_{\text{kineticheatflowdissipation}} - \underbrace{\frac{\mathbf{q}_c}{\theta_c^2}\cdot\nabla\theta_c}_{\text{configurationalheatflowdissipation}} \geq 0 \tag{28}$$

From Eq. (28), the total dissipation can be divided into four parts, i.e., inelastic dissipation, dissipation resulting from the energy exchange between two subsystems, and kinetic and configurational heat flow dissipation. Here we assume that these four parts of dissipation are independent of one another. Then the following inequalities can be obtained from Eq. (28), which are stronger than the requirement of nonnegative intrinsic dissipation, i.e.,

$$\left(\frac{\overline{\mathbf{T}}_{dis}}{\theta_k}+\frac{\overline{\mathbf{T}}_{sto}}{\theta_c}\right) : \mathbf{D}^p - \frac{1}{\theta_c}\frac{\partial \psi_c}{\partial \gamma}\dot{\gamma} \geq 0 \tag{29a}$$

$$q_{ck}\left(\frac{1}{\theta_k}-\frac{1}{\theta_c}\right) \geq 0 \tag{29b}$$

$$-\frac{\mathbf{q}_k}{\theta_k^2}\cdot\nabla\theta_k \geq 0 \tag{29c}$$

$$-\frac{\mathbf{q}_c}{\theta_c^2}\cdot\nabla\theta_c \geq 0 \tag{29d}$$

2.5. Free energy density and specific constitutive functions

For simplicity, thermal expansion is not taken into consideration since the temperature rise resulting from deformation has a slight effect on the elastic deformation of metallic glasses. With the definition of $\mathbf{E}^e = \frac{1}{2}\ln \mathbf{C}^e = \ln\mathbf{U}^e$, the form of the kinetic Helmholtz free energy per unit reference volume can be assumed to be

$$\psi_k = c_k\left\{\left(\theta_k-\theta_k^0\right) - \theta_k\log\left(\theta_k/\theta_k^0\right)\right\} + \mu\left|\mathbf{E}_0^e\right|^2 + \frac{1}{2}k\{\mathrm{tr}(\mathbf{E}^e)\}^2 \tag{30}$$

where $c_k = \widehat{c}_k(\theta_k,\theta_c)$ is the kinetic specific heat per unit reference volume; θ_k^0 is the reference kinetic temperature; and the shear and bulk moduli are denoted by $\mu = \widehat{\mu}(\theta_k)$ and $k = \widehat{k}(\theta_k)$, respectively.

The purely configurational thermal contribution to the configurational free energy density is the same as the purely kinetic thermal contribution to the kinetic free energy density. In addition, a shear transformation hardening energy is introduced to characterize the constraint of the neighboring matrix on the shear transformation. Thus, we can assume that the form of configurational free energy density is

$$\psi_c = c_c\left\{\left(\theta_c - \theta_c^0\right) - \theta_c \log\left(\theta_c / \theta_c^0\right)\right\} + \chi\gamma \tag{31}$$

where $c_c = \widehat{c}_c(\theta_k, \theta_c)$ is the configurational specific heat per unit reference volume, θ_c^0 is the reference configurational temperature, and $\chi = \widehat{\chi}(\theta_k, \theta_c, \gamma)$ is a physical quantity analogous to the back stress.

Substituting Eq. (30) into Eq. (27a) yields

$$\mathbf{T}^* = 2\mu\mathbf{E}_0^e + k \cdot \mathrm{tr}(\mathbf{E}^e)\mathbf{1} \tag{32}$$

Combining Eqs. (18a), (18b) and Eq. (32), it can be obtained that

$$\overline{\mathbf{T}} = \mathbf{U}^e\mathbf{T}^*\mathbf{U}^{e-1} = \mathbf{T}^* \tag{33}$$

Substituting Eq. (31) into Eq. (29a) yields

$$\left(\frac{\overline{\mathbf{T}}_{dis}}{\theta_k} + \frac{\overline{\mathbf{T}}_{sto}}{\theta_c}\right) : \mathbf{D}^p - \frac{1}{\theta_c}\chi\dot{\gamma} \geq 0 \tag{34}$$

Following the work of Thamburaja and Ekambaram (2007), we assume that the inelastic stretching tensor can be expressed as

$$\mathbf{D}^p = \sqrt{\frac{1}{2}}\dot{\gamma}\mathbf{N} \tag{35}$$

where $\mathbf{N}$ is the inelastic flow direction, which satisfies $\mathrm{tr}(\mathbf{N}) = 0$ and $\| \mathbf{N} \| = 1$. Hereafter, $\mathrm{tr}(\bullet)$ denotes the trace of the second-order tensor $\bullet$.

Substituting Eq. (35) into Eq. (34),

$$\left[\sqrt{\frac{1}{2}}\left(\frac{\overline{\mathbf{T}}_{dis}}{\theta_k} + \frac{\overline{\mathbf{T}}_{sto}}{\theta_c}\right) : \mathbf{N} - \frac{1}{\theta_c}\chi\right]\dot{\gamma} \geq 0 \tag{36}$$

Inequality (36) is tenable if

$$\sqrt{\frac{1}{2}}\left(\frac{\overline{\mathbf{T}}_{dis}}{\theta_k} + \frac{\overline{\mathbf{T}}_{sto}}{\theta_c}\right) : \mathbf{N} - \frac{1}{\theta_c}\chi = \widehat{H} \tag{37}$$

with the function $\widehat{H}$ satisfying $\mathrm{sign}(\widehat{H}) = \mathrm{sign}(\dot{\gamma})$.

Assuming a special situation in which $\theta_k = \theta_c = \theta$ is satisfied, Eq. (37) can be rewritten as

$$\sqrt{\frac{1}{2}}\overline{\mathbf{T}} : \mathbf{N} = \widehat{H}\theta + \chi \tag{38}$$

To satisfy Eq. (38), we let

$$\mathrm{dev}(\overline{\mathbf{T}}) = \sqrt{2}(\widehat{H}\theta + \chi)\mathbf{N} \tag{39}$$

where $\mathrm{dev}(\bullet)$ is the deviatoric portion of the second-order tensor $\bullet$. At this point, it can be assumed that Eq. (39) is always tenable since $\| \mathbf{N} \| = 1$. Then it can be obtained that

$$\mathbf{N} = \frac{\mathrm{dev}(\overline{\mathbf{T}})}{\| \mathrm{dev}(\overline{\mathbf{T}}) \|} \tag{40}$$

Substituting Eq. (40) into Eq. (37),

$$\left[\left(\frac{1}{\theta_k} - \frac{1}{\theta_c}\right)\overline{\mathbf{T}}_{dis} + \frac{\overline{\mathbf{T}}}{\theta_c}\right] : \frac{\mathrm{dev}(\overline{\mathbf{T}})}{\| \mathrm{dev}(\overline{\mathbf{T}}) \|} = \sqrt{2}\left(\widehat{H} + \frac{1}{\theta_c}\chi\right) \tag{41}$$

To satisfy Eq. (41), we can assume that

$$\left(\frac{1}{\theta_k} - \frac{1}{\theta_c}\right)\mathrm{dev}(\overline{\mathbf{T}}_{dis}) = \sqrt{2}\left(\widehat{H} + \frac{1}{\theta_c}\chi\right)\frac{\mathrm{dev}(\overline{\mathbf{T}})}{\| \mathrm{dev}(\overline{\mathbf{T}}) \|} - \frac{\mathrm{dev}(\overline{\mathbf{T}})}{\theta_c} \tag{42}$$

If Eq. (42) is always satisfied, the following relations can be given:

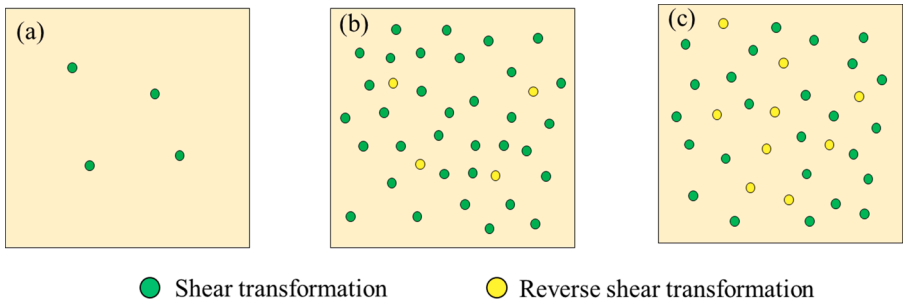

Fig. 2. Evolution of shear transformation sites and its resulting in reverse shear transformation sites with the increase of applied strain: (a) in the early stage of deformation, only little shear localization occurs; (b) in the stage of strain softening, many STZs are activated, and few inverse shear transformations occurs; (c) in the steady stage, the shear transformations and reverse ones are at a quasi-equilibrium.

$$\mathbf{N} = \frac{\mathrm{dev}(\overline{\mathbf{T}})}{\parallel \mathrm{dev}(\overline{\mathbf{T}}) \parallel} = \frac{\mathrm{dev}(\overline{\mathbf{T}}_{dis})}{\parallel \mathrm{dev}(\overline{\mathbf{T}}_{dis}) \parallel} = \frac{\mathrm{dev}(\overline{\mathbf{T}}_{sto})}{\parallel \mathrm{dev}(\overline{\mathbf{T}}_{sto}) \parallel} \tag{43}$$

Substituting Eq. (43) into Eq. (37), it can be obtained that

$$\widehat{H} = \left(\frac{\overline{\tau}_{dis}}{\theta_k} + \frac{\overline{\tau}_{sto}}{\theta_c}\right) - \frac{1}{\theta_c}\chi \tag{44}$$

where $\overline{\tau}_{dis} = \sqrt{\frac{1}{2}} \parallel \mathrm{dev}(\overline{\mathbf{T}}_{dis}) \parallel$ and $\overline{\tau}_{sto} = \sqrt{\frac{1}{2}} \parallel \mathrm{dev}(\overline{\mathbf{T}}_{sto}) \parallel$ are the von Mises equivalent shear stresses of the dissipation stress and storage stress, respectively.

STZ has been famous as a unit plastic event of amorphous solids. However, along with shear transformation, a strain energy field would be produced and accumulated with an increase in the local inelastic deformation due to the constraint of the matrix on the shear transformation zone. Finally, such a strain energy field would result in a reverse shear transformation so that the stored energy can be released, as shown in Fig. 2. The classical shear transformation zone theory does not consider the relaxation of such stored energy, which is in the form of inverse shear transformation. Here the classical shear transformation zone theory is developed to describe the contributions of both shear transformation and inverse shear transformation. According to transition state theory, the evolution equation of inelastic shear strain in a local region can be given as

$$\dot{\gamma} = \dot{\gamma}_0 \left[\underbrace{\exp\left(\frac{-\Delta G}{k_b\theta_k}\left(1 - \left(\frac{\tau}{\tau_0}\right)^p\right)^q\right)}_{\mathrm{Probability of shear transformation}} - \underbrace{\exp\left(\frac{-1}{k_b\theta_k}\left(\Delta G\left(1 + \left(\frac{\tau}{\tau_0}\right)^p\right)^q - S\Omega\right)\right)}_{\mathrm{Probability of reverse shear transformation}} \right] \tag{45}$$

where $\dot{\gamma}_0 = \dot{\widehat{\gamma}}_0(\theta_c) \geq 0$ represents the reference plastic strain rate when the shear transformation is activated, which is related to the degree of configuration disorder, $\Delta G = \Delta\widehat{G}(\theta_k)$ is the activation energy barrier without the applied stress, which has a sudden change near the glass transition temperature, $k_b\theta_k$ is the kinetic thermal energy of the system, τ_0 is the thermally activated stress, and p and q are model parameters that are defined by the obstacle profile. And it is satisfied that the conditions $0 \leq p \leq 1$ and $1 \leq q \leq 2$ are satisfied; for simplicity, we set $p = 1$ and $q = 1$. $S = \widehat{S}(\dot{\gamma}, \theta_k, \theta_c)$ is the locally stored transformation energy, which is caused by the shear transformation and results in the reverse shear transformation. Ω is the volume of a shear transformation zone, and τ is the driving force of shear transformation. Some experimental results have shown that the deformation of metallic glass is dependent on the hydrostatic pressure (Greer, 2013); here, we define the driving force as

$$\tau = \overline{\tau} - \phi P \tag{46}$$

where $\overline{\tau} = \sqrt{\frac{1}{2}} \parallel \mathrm{dev}(\overline{\mathbf{T}}) \parallel$ is the equivalent shear stress, $P = -\frac{1}{3}\mathrm{tr}(\overline{\mathbf{T}})$ is the hydrostatic pressure, and ϕ is the pressure-sensitivity parameter, which satisfies the condition $0 \leq \phi \leq 1$.

In general, the shear transformation is an ephemeral, noise-activated, and configurational fluctuation. However, in a local region of metallic glass, the state of the microstructure is always certain at the current time and can be characterized by the configurational temperature. Thus, Shi et al. (2007) think of the shear transformation as infrequent events and the correspondingly long time scales associated with plastic deformation can be determined by configurational temperature through a Boltzmann-like factor. Then the reference plastic strain rate can be expressed as

$$\dot{\gamma}_0 = \Delta\gamma_0 \nu_0 \exp\left(-\frac{\Delta G}{k_b\theta_c}\right) \tag{47}$$

where $\Delta\gamma_0$ is the strain increment for a time of shear rearrangement; ν_0 is the attempt frequency for shear transformation; and $\exp\left(-\frac{\Delta G}{k_b\theta_c}\right)$ is a Boltzmann-like factor.

Following the work of Hasan and Boyce (2010), the rate of locally stored transformation energy can be given as

$$\dot{S} = \beta\tau\dot{\gamma} - \beta_0\omega S \tag{48}$$

where $\beta = \widehat{\beta}(\gamma)$ is a variation of the parameter that informs the rate of storage of inelastic work falling off with an increase in the inelastic strain; following the work of Hasan and Boyce (2010), we set $\beta = \beta_1[1 - \beta_2\exp(-\beta_3\gamma)]$, where β_1, β_2 and β_3 are the material parameters, β_0 is a material parameter that is related to the recovery of locally stored transformation energy, and ω is an effective frequency relating to shear transformations; here we assume that it is equal to the frequency of reverse shear transformation; then, the evolution equation of ω is given as

$$\omega = \nu_0\exp\left(-\frac{\Delta G}{k_b\theta_c}\right)\exp\left(-\frac{\Delta G}{k_b\theta_k}\left(1+\left(\frac{\tau}{\tau_0}\right)^p\right)^q\right)\exp\left(\frac{S\Omega}{k_b\theta_k}\right) \tag{49}$$

Now, let us briefly discuss the physical meaning of Eq. (48). The evolution of the locally stored transformation energy is the result of two competing effects: an increase attributed to the partial storage of the inelastic work of deformation and a decrease due to the recovery phenomena. While the first effect dominates during the initial stages of deformation, once the value of the locally stored transformation strain energy is sufficiently large, secondary relaxation events begin to occur at an appreciable rate, and the value of S falls somewhat: during steady-state flow conditions, the two effects virtually cancel each other out, resulting in no net change in the value of S.

As mentioned above, both shear transformation and reverse shear transformation may occur in metallic glass. Now, let us imagine a situation in which a high stress is applied and kept for a period of time and then unloaded to zero. At this moment, since there is no external force to drive shear transformation and a large strain energy field has been stored up in the material, the reverse shear transformation rate is larger than the shear transformation rate. From Eq. (45) it is determined that $\dot{\gamma} < 0$. In fact, whether $\dot{\gamma}$ is positive or negative is only determined by the competition between the shear transformation and reverse shear transformation. If the occurrence frequency of shear transformation is larger than that of the reverse shear transformation per unit time, $\dot{\gamma} > 0$; otherwise, $\dot{\gamma} \le 0$. To quantitatively estimate whether $\dot{\gamma}$ is positive or negative, a quantitative criterion should be provided. In fact, deeply analyzing Eq. (45), it is not difficult to determine that

$$\left(\overline{\tau} - \phi P - \frac{S\Omega}{2\Delta G}\tau_0\right)\dot{\gamma} \ge 0 \tag{50}$$

is always tenable.

Let us review Eq. (36), where it is constrained that $\mathrm{sign}(\widehat{H}) = \mathrm{sign}(\dot{\gamma})$. To satisfy the second law of thermodynamics, we set

$$\widehat{H} = \left(\frac{\overline{\tau}_{dis}}{\theta_k} + \frac{\overline{\tau}_{sto}}{\theta_c} - \frac{1}{\theta_c}\chi\right) = \lambda\left(\overline{\tau} - \phi P - \frac{S\Omega}{2\Delta G}\tau_0\right) \tag{51}$$

where $\lambda = \widehat{\lambda}(\theta_k, \theta_c) \ge 0$ is a material coefficient.

Assuming that only the hydrostatic pressure is applied, Eq. (51) can be rewritten as

$$\frac{1}{\theta_c}\chi = \lambda\left(\phi P + \frac{S\Omega}{2\Delta G}\tau_0\right) \tag{52}$$

From Eq. (52), it can be defined that

$$\chi = \theta_c\lambda\left(\phi P + \frac{S\Omega}{2\Delta G}\tau_0\right) \tag{53}$$

Substituting Eq. (53) into Eq. (51), it can be obtained that

$$\left(\frac{\overline{\tau}_{dis}}{\theta_k} + \frac{\overline{\tau}_{sto}}{\theta_c}\right) = \lambda\overline{\tau} \tag{54}$$

Since this is satisfied with $\overline{\tau}_{dis} + \overline{\tau}_{sto} = \overline{\tau}$,

$$\overline{\tau}_{dis} = \frac{\theta_k(\lambda\theta_c - 1)}{\theta_c - \theta_k}\overline{\tau} \ge 0 \tag{55a}$$

$$\overline{\tau}_{sto} = \frac{\theta_c(1 - \lambda\theta_k)}{\theta_c - \theta_k}\overline{\tau} \ge 0 \tag{55b}$$

Since both $\overline{\tau}_{dis}$ and $\overline{\tau}_{sto}$ must be greater than or equal to zero, so it can be determined from Eq. (55a, b) that

Table 1
The main equations of the proposed model.

Decomposition of the deformation
$\mathbf{F} = \mathbf{F}^e\mathbf{F}^p$, $\mathbf{F}^e = \mathbf{R}^e\mathbf{U}^e$, $\mathbf{F}^e = \mathbf{R}^e\mathbf{U}^e$
$\mathbf{L} = \mathbf{L}^e + \mathbf{F}^e\mathbf{L}^p\mathbf{F}^{e-1}$, $\mathbf{L}^e = \dot{\mathbf{F}}^e\mathbf{F}^{e-1}$, $\mathbf{D}^e = \frac{1}{2}(\mathbf{L}^e + \mathbf{L}^{e\mathrm{T}})$
$\mathbf{W}^e = \frac{1}{2}(\mathbf{L}^e - \mathbf{L}^{e\mathrm{T}})$, $\mathbf{D}^p = \mathbf{L}^p = \dot{\mathbf{F}}^p\mathbf{F}^{p-1}$, $\mathbf{D}^p = \sqrt{\frac{1}{2}}\dot{\gamma}\mathbf{N}$
$\mathbf{E}^e = \frac{1}{2}\ln \mathbf{C}^e = \ln\mathbf{U}^e$
Elastic constitutive relation
$\overline{\mathbf{T}} = \mathbf{T}^* = 2\mu\mathbf{E}_0^e + k \cdot \mathrm{tr}(\mathbf{E}^e)\mathbf{1}$
The evolution equation of inelastic flow rate
$\dot{\gamma} = \Delta\gamma_0\nu_0\exp\left(-\frac{\Delta G}{k_b\theta_c}\right)\left[\exp\left(\frac{-\Delta G}{k_b\theta_k}\left(1 - \left(\frac{\tau}{\tau_0}\right)\right)\right) - \exp\left(\frac{-\Delta G}{k_b\theta_k}\left(1 + \left(\frac{\tau}{\tau_0}\right)\right)\right)\exp\left(\frac{S\Omega}{k_b\theta_k}\right)\right]$
Where
$\tau = \overline{\tau} - \phi P$, $\overline{\tau} = \sqrt{\frac{1}{2}}\parallel \mathrm{dev}(\overline{\mathbf{T}}) \parallel$, $P = -\frac{1}{3}\mathrm{tr}(\overline{\mathbf{T}})$
The inelastic flow direction
$\mathbf{N} = \frac{\mathrm{dev}(\overline{\mathbf{T}})}{\parallel \mathrm{dev}(\overline{\mathbf{T}})\parallel}$
The evolution equation of locally stored transformation energy
$\dot{S} = \beta\tau\dot{\gamma}^p - \beta_0\omega S$
Where
$\beta = \beta_1[1 - \beta_2\exp(-\beta_3\gamma^p)]$
$\omega = \nu_0\exp\left(-\frac{\Delta G}{k_b\theta_c}\right)\exp\left(-\frac{\Delta G}{k_b\theta_k}\left(1 + \left(\frac{\tau}{\tau_0}\right)\right)\right)\exp\left(\frac{S}{k_b\theta_k}\right)$
The evolution equations of the kinetic and configurational temperatures
$c_k\dot{\theta}_k = \overline{\tau}_{dis}\dot{\gamma} + \kappa_k\Delta\theta_k + q_k + \kappa_{ck}[\exp(-\Delta G/k_b\theta_c) - \exp(-\Delta G/k_b\theta_k)]$
$c_c\dot{\theta}_c = \overline{\tau}_{sto}\dot{\gamma} - \chi\dot{\gamma} + \kappa_c\Delta\theta_c - \kappa_{ck}[\exp(-\Delta G/k_b\theta_c) - \exp(-\Delta G/k_b\theta_k)]$
$\overline{\tau}_{dis} = \frac{\theta_k}{\theta_c+\theta_k}\overline{\tau}$, $\overline{\tau}_{sto} = \frac{\theta_c}{\theta_c+\theta_k}\overline{\tau}$, $\chi = \frac{2\theta_c}{\theta_c+\theta_k}\left(\phi P + \frac{S\Omega}{2\Delta G}\tau_0\right)$

$$\frac{1}{\theta_c} \le \lambda \le \frac{1}{\theta_k} \tag{56}$$

To always satisfy Eq. (56), it can be assumed that

$$\lambda = \frac{2}{\theta_c + \theta_k} \tag{57}$$

Substituting Eq. (57) into Eq. (55a, b),

$$\overline{\tau}_{dis} = \frac{\theta_k}{\theta_c + \theta_k}\overline{\tau} \tag{58a}$$

$$\overline{\tau}_{sto} = \frac{\theta_c}{\theta_c + \theta_k}\overline{\tau} \tag{58b}$$

Substituting Eq. (57) into Eq. (53) yields

$$\chi = \frac{2\theta_c}{\theta_c + \theta_k}\left(\phi P + \frac{S\Omega}{2\Delta G}\tau_0\right) \tag{59}$$

From Eq. (59), it can be determined that the back stress-like term is closely related to the driving force for inverse shear transformation.

2.6. Balance of energy

Substituting Eq. (30) into Eq. (27b) yields

$$\eta_k = -\frac{\partial\psi_k}{\partial\theta_k} = c_k\log\left(\theta_k / \theta_k^0\right) \tag{60}$$

Similarly, substituting Eq. (31) into Eq. (27c) yields

$$\eta_c = -\frac{\partial\psi_c}{\partial\theta_c} = c_c\log\left(\theta_c / \theta_c^0\right) \tag{61}$$

Assuming that both the kinetic and configurational subsystems obey Fourier's law of heat conduction, inequalities (29c) and (29d)

are always satisfied if the following is set:

$$\mathbf{q}_k = -\kappa_k \nabla \theta_k \tag{62a}$$

$$\mathbf{q}_c = -\kappa_c \nabla \theta_c \tag{62b}$$

Here, $\kappa_k = \widehat{\kappa}_k(\theta_k, \theta_c)$ and $\kappa_c = \widehat{\kappa}_c(\theta_k, \theta_c)$ are the coefficients of kinetic and configurational thermal conduction, respectively.

Referring to the work of Shi et al. (2007), it is assumed that the energy exchange between the two subsystems obeys the binary annihilation function relation. It can then be set as

$$q_{ck} = \kappa_{ck}[\exp(-\Delta G / k_b\theta_c) - \exp(-\Delta G / k_b\theta_k)] \tag{63}$$

where $\kappa_{ck} = \widehat{\kappa}_{ck}(\theta_k, \theta_c) \geq 0$ are the coefficients of energy exchange.

Substituting Eq. (63) into Eq. (29b) yields

$$\kappa_{ck}[\exp(-\Delta G / k_b\theta_c) - \exp(-\Delta G / k_b\theta_k)]\frac{\theta_c - \theta_k}{\theta_k\theta_c} \geq 0 \tag{64}$$

It is not difficult to prove that inequality (64) is always tenable.

From Eqs. (19a), 21a), ((30), (32), (33), (35), (43), 58a), ((60), 62a) and ((63), it can be determined that

$$c_k\dot{\theta}_k = \overline{\tau}_{dis}\dot{\gamma} + \kappa_k\Delta\theta_k + q_k + \kappa_{ck}[\exp(-\Delta G / k_b\theta_c) - \exp(-\Delta G / k_b\theta_k)] \tag{65}$$

From Eqs. (19b), 21b), ((31), (33), (35), (43), 58b), ((61), 62b) and ((63), it can be determined that

$$c_c\dot{\theta}_c = \overline{\tau}_{sto}\dot{\gamma} - \chi\dot{\gamma} + \kappa_c\Delta\theta_c - \kappa_{ck}[\exp(-\Delta G / k_b\theta_c) - \exp(-\Delta G / k_b\theta_k)] \tag{66}$$

Eqs. (65) and (66) give the evolution equations of the kinetic and configurational temperatures, respectively.

So far, the constitutive model for metallic glass based on out-of-equilibrium statistical concepts has been established. The main equations of the proposed model are listed in Table 1.

A time-integration procedure for our developed constitutive model has been proposed and implemented into a finite element code as a user material subroutine (UMAT) by using an implicit integration scheme in this work. It should be noted that the solution of configurational thermal diffusion term is the difficult point; here, the method from the work of Qu (2004) was adopted to solve the value of $\Delta\theta_c$.

3. Determination of the material parameters

Lu (2002) systematically conducted a series of uniaxial monotonic compressive experiments on a Vitreloy 1 metallic glass under different strain rates (from quasi-static to dynamic) and ambient temperatures (from room temperature to supercooled liquid region). In this work, we adopt the newly developed constitutive model to predict the experiments (e.g., deformations under different strain rates and ambient temperatures) conducted by Lu (2002). To further validate the predictive capability of the new constitutive model, the shear localization of metallic glass during quasi-static monotonic tensile deformation is also modeled. In these simulations, part of the set of constitutive parameters or function relations in this constitutive model are obtained from the literature, and the others are determined through the trial-and-error method from the experimental results on the compressive deformations from Lu (2002).

From the experimental results, it can be determined that the elastic modulus of the amorphous solid is dependent on the kinetic temperature; close to the glass transition temperature, such a temperature correlation becomes increasingly stronger. Following the work of Srivastava et al. (2010), it can be set as

$$\mu = \frac{1}{2}\left(\mu^g + \mu^l\right) - \frac{1}{2}\left(\mu^g - \mu^l\right)\tanh\left(\frac{\theta_k - \theta_g}{\vartheta}\right) \tag{67a}$$

$$k = \frac{1}{2}\left(k^g + k^l\right) - \frac{1}{2}\left(k^g - k^l\right)\tanh\left(\frac{\theta_k - \theta_g}{\vartheta}\right) \tag{67b}$$

where μ^g and k^g are the shear and bulk moduli of the glassy state, respectively, μ^l and k^l are the shear and bulk moduli in the supercooled liquid region, respectively, θ_g is the glass transition temperature, and ϑ is a parameter related to the temperature range across which the transition occurs. The glass transition temperature of Vitreloy 1 metallic glass is determined to be $\theta_g = 625$Kin the work of Lu (2002). Through fitting to the simple compression experiments of Lu (2002), $\mu^g = 35.29$GPa, $k^g = 114.29$GPa, $\mu^l = 1.47$GPa, $k^l = 4.76$GPa and $\vartheta = 42$K.

As discussed in the work of Han et al. (2020), the activation energy is found to change dramatically at the glass-to-liquid transition. Thus, it is set as

$$\Delta G = \frac{1}{2}\left(\Delta G^g + \Delta G^l\right) - \frac{1}{2}\left(\Delta G^g - \Delta G^l\right)\tanh\left(\frac{\theta_k - \theta_g}{\vartheta}\right) \tag{68}$$

where ΔG^g is the activation energy of the glassy state and ΔG^l is the activation energy in the supercooled liquid region. In the glassy

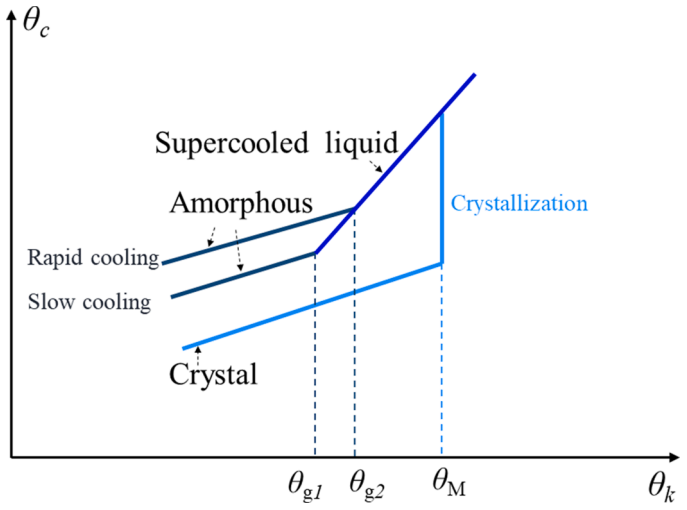

Fig. 3. The evolution of configurational temperature with the decrease of kinetic temperature during the quenching process.

state, some 2-D molecular dynamic simulations show that the activation energy is 0.5ev to 0.95ev (Greer et al., 2013; Han et al., 2020); here, it is set as $\Delta G^g = 0.712$ev through fitting to match the experimental data. In the supercooled liquid region, the activation energy is much less than 0.5ev (Han et al., 2020); here, it is taken as $\Delta G^l = 0.212$ev through fitting to match the experimental data.

For a Vitreloy 1 metallic glass, the strain increment $\Delta\gamma_0$ and the volume of the shear transformation zone Ω are constants. In the work of Jiang and Dai (2009), $\Delta\gamma_0 = 0.1$ and $\Omega = 2\text{nm}^3$are set; here, they are also taken as the values. The attempt frequency for shear transformation ν_0 is dependent on the temperature. For simplification, we assume it to be a constant; through fitting to match the experimental data, it is set as $\nu_0 = 1 \times 10^3 s^{-1}$.

β_1, β_2 and β_3 are the material parameters related to the rate of storage of inelastic work falling off with an increase in the inelastic strain; referring to the work of Hasan and Boyce (2010), they are set as $\beta_1 = 0.01$, $\beta_2 = 1$ and $\beta_3 = 1800$, where β_0 is a material parameter that is related to the recovery of locally stored transformation energy; in the work of Hasan and Boyce (2010), they set $\beta_0 = 1$; here, it is also taken as $\beta_0 = 1$.

The model parameters p and q are the fitting parameters. Referring to the work of Orowan (1940), they are set as $p = 1$ and $q = 1$ in Section 2. The thermally activated stress τ_0 is related to the yielding stress; by fitting the compressive stress–strain curve at room temperature given by Lu (2002), it is taken as $\tau_0 = 1155$MPa. For simplicity, here the effect of hydrostatic pressure is neglected based on the work of Huang and Suo (2002); thus, it is set as $\phi = 0$.

As discussed in the work of Kamrin and Bouchbinder (2014), the configurational specific heat capacity c_c is dependent on the kinetic and configurational temperature; here it is taken as

$$c_c = c_{c0}\frac{\Delta G}{k_b(\theta_\infty - \theta_c)} \tag{69}$$

Here c_{c0} is the reference configurational specific heat capacity; by the trial-and-error method from the experimental results on the compressive deformation of Lu (2002), it is set as $c_{c0} = 0.002\text{MJ}/\text{m}^3\text{K}$, where θ_∞ is the saturation value of the configurational temperature. As is known, the configuration is gradually loosened when the metallic glass is molten. At this moment, the configurational disorder has little effect on its deformation. Thus, we consider that the maximal configurational disorder is slightly higher than the melting point temperature. In the work of Lu (2002), the melting point temperature of Vitreloy 1 metallic glass is 993 K; here, it can be taken as $\theta_\infty = 1025$K.

As mentioned above, the coefficient of energy exchange κ_{ck} is a function of the kinetic and configurational temperatures. Following the work of Shi et al. (2007), it is taken as

$$\kappa_{ck} = \kappa_0 c_c \exp(-\Delta G / k_b\theta_c) \tag{70}$$

where κ_0 is a constant; by fitting one of the compressive stress–strain curves, it is set as $\kappa_0 = 200\text{K}/\text{s}$ in this work.

As discussed in the work of Shi et al. (2007), there is a statistical linear correlation between the configurational temperature and the free volume concentration. Thus, we set $\kappa_c = c_c D$, where D is the diffusivity of the free volume concentration in the work of Huang and Suo (2002). Following their work, it is set as $D = 3.23\text{nm}^2/\text{s}$.

Metallic glass is also called a frozen liquid. At the crystallization temperature, the configuration rearrangement is not complete; instead, the liquid metal solidifies directly. This indicates that the configuration does not undergo a sudden jump, which is different from that of crystalline materials. Fig. 3 shows a sketch map between the configurational temperature and the kinetic temperature. From Fig. 3, it can be set as

Table 2
Material parameters for metallic glass using in this work.

Elastic parameter
$E^g = 50\text{GPa}$, $E^l = 46\text{GPa}$, $\nu = 0.36$, $\vartheta = 42\text{K}$, $T_g = 625\text{K}$
Parameters related to shear transformation
$\Delta\gamma_0 = 0.1$, $\nu_0 = 1\times10^3\text{s}^{-1}$, $\Delta G^g = 0.712\text{ev}$, $\Delta G^l = 0.212\text{ev}$, $\Omega = 2\text{nm}^3$
$\phi = 0$, $\beta_0 = 1$, $\beta_1 = 0.01$, $\beta_2 = 1$, $\beta_3 = 1800$, $Y_0 = 1.155\text{GPa}$
$k_b = 1.38\times10^{-23}\text{J/K}$
Parameters related to configurational temperature
$c_{c0} = 0.002\text{MJ/m}^3\text{K}$, $\kappa_0 = 200\text{MPa/s}$, $\kappa_c = 3.23\text{nm}^2/\text{s}$, $\theta_\infty = 1025\text{K}$, $\theta_k^c = 703\text{K}$, $\alpha = 0.8$
Parameters related to kinetic temperature
$c_k = 0.8\text{MJ/m}^3\text{K}$, $\kappa_k = 11\text{J/(K}\cdot s)$

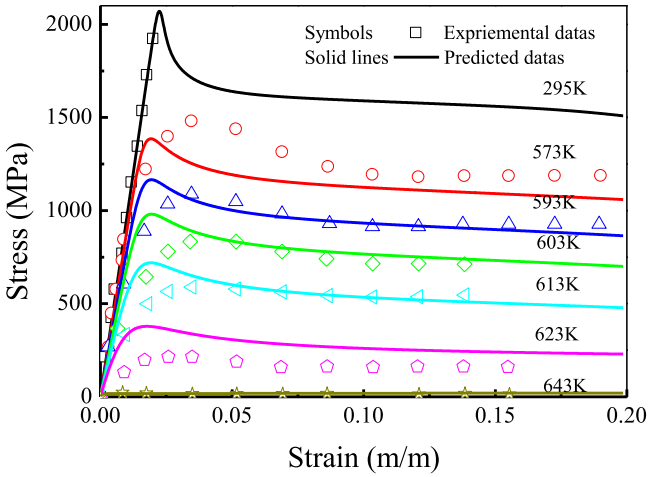

Fig. 4. The predicted and experimental stress-strain curves of metallic glass during compressive deformations under the ambient temperatures from 295K to 643K and applied strain rate of $1\times10^{-4}s^{-1}$ (Lu, 2002).

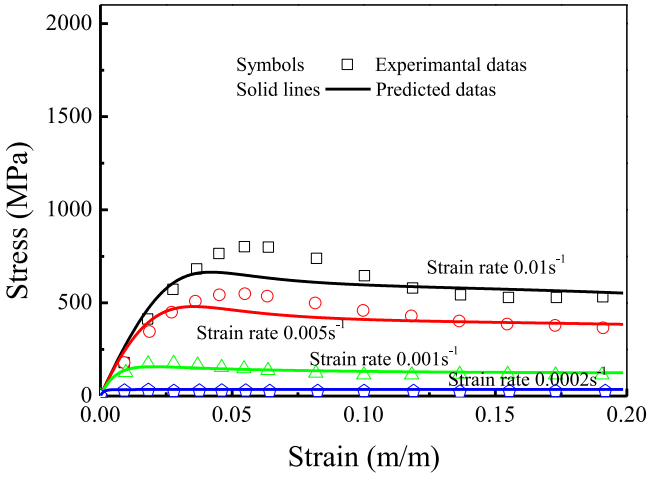

Fig. 5. The predicted and experimental stress-strain curves of metallic glass during compressive deformations under the ambient temperature of 643K and applied strain rates from $2\times10^{-4}s^{-1}$ to $1\times10^{-2}s^{-1}$ (Lu, 2002).

$$\theta_c^0 = \theta_\infty - \left(\theta_k^c - \theta_k\right) - \alpha\left(\theta_k^c - \theta_g\right) + \alpha\langle\theta_k - \theta_g\rangle, \tag{71}$$

where θ_k^c is the crystallization temperature (Lu (2002) sets $\theta_k^c = 703\text{K}$), and α is the dimensionless coefficient, which is set as $\alpha = 0.8$.

The kinetic specific heat capacity and the coefficients of kinetic thermal conduction are dependent on the kinetic and configurational temperatures. For simplicity, here we assume that the values for these two material parameters are constant. Referring to the

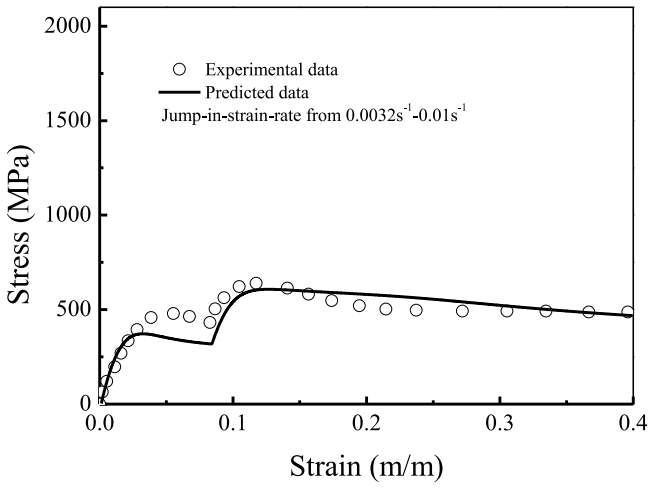

(a)

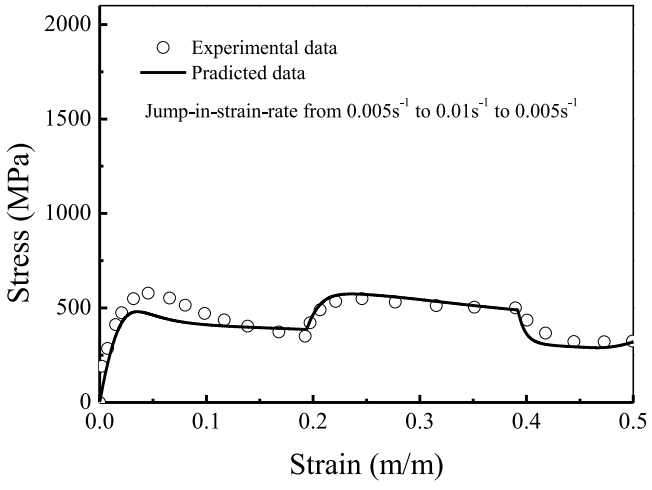

(b)

Fig. 6. The predicted and experimental compressive stress-strain curves for a jump-in-strain-rate experiment from a strain rate of (a) $3.2 \times 10^{-3} s^{-1}$ to $1 \times 10^{-2} s^{-1}$, and (b) $5 \times 10^{-3} s^{-1}$ to $1 \times 10^{-2} s^{-1}$ and back $5 \times 10^{-3} s^{-1}$. Both the two experiments are conducted at the ambient temperature of 643K (Lu, 2002).

work of Jiang and Dai (2009) and Thamburaja and Ekambaram (2007), they are taken as $c_k = 0.8\text{MJ}/\text{m}^3\text{K}$ and $\kappa_k = 11\text{W}/\text{mK}$.

All the values for the material parameters used in this work are listed in Table 2, unless noted otherwise.

4. Simulation and discussion

In this section, we firstly model some macroscopic deformations of metallic glass under different strain rates and ambient temperatures provided by Lu (2002), and compare the predicted stress-strain curves with the corresponding experimental ones to validate the effectiveness of the developed model. Then, based on the simulations, we discuss the origin of deformation mode during the deformation of metallic glass under different applied conditions. Finally, small scale finite element models are constructed to simulate the local deformation of metallic glass so that the initiation and propagation of shear bands can be captured.

4.1. Macroscopic deformations

From the work of Thamburaja and Ekambaram (2007), it is determined that the deformation of metallic glass is relatively homogeneous when the strain rate is small (i.e., 1×10^{-4} s^{-1}) and the ambient temperature is close to the glass transition temperature, or

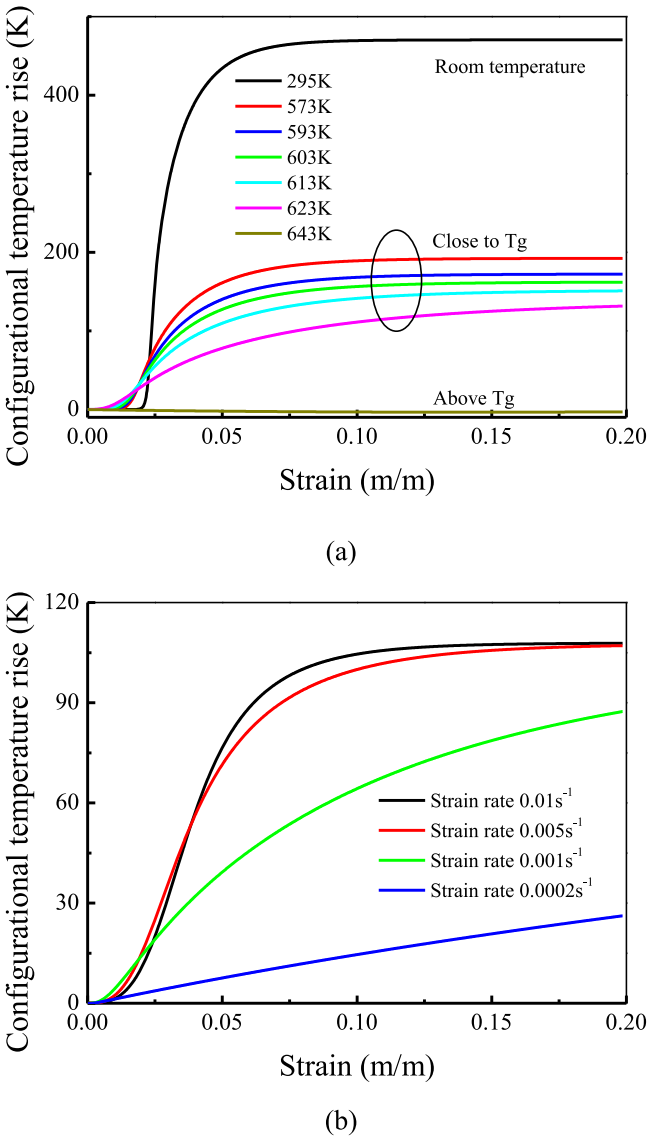

Fig. 7. The configurational temperature-applied strain during the compressive deformation under (a) the ambient temperatures from 295K to 643K and applied strain rate of $1 \times 10^{-4}s^{-1}$, and (b) the ambient temperature of 643K and applied strain rates from $2 \times 10^{-4}s^{-1}$ to $1 \times 10^{-2}s^{-1}$.

the strain rate is applied from 1×10^{-4} s^{-1} to 3.2×10^{-2} s^{-1}, but the ambient temperature is larger than the glass transition temperature. In addition, the shear localization has little effect on the overall stress–strain responses of metallic glasses before failure occurs, since the shear localization is only constrained within narrow bands whose size is much smaller than the size of samples in the work of Lu (2002). Thus, we use a three-dimensional finite element model with only one finite element to model the deformations of metallic glass in this section. To capture the evolution of the kinetic temperature in the stage of deformation, the C3D8T finite element is adopted.

To prove the effectiveness of the newly developed constitutive model in predicting the deformations of metallic glass, the quasi-static deformations (the strain rate is 1×10^{-4} s^{-1}) of metallic glass from room temperature (295 K) to the supercooled liquid region (643 K) are predicted. Fig. 4 shows a comparison of the predicted overall stress–strain curves with the corresponding experimental curves. The comparison results show that the predicted results are in good agreement with the experimental results. This indicates that the new constitutive model can well predict the deformations of metallic glass under different ambient temperatures.

To further demonstrate the reasonability of the proposed constitutive model in describing the deformations of metallic glass under different applied strain rates, we also simulate the deformations of metallic glass under 643 K and strain rates from 2×10^{-4} s^{-1} to 1×10^{-2} s^{-1}. Fig. 5 shows the modeled stress–strain curves and their corresponding experimental curves. It can be seen from the comparison results that the modeling results agree well with the corresponding experiments. Thus, it can be concluded that the new constitutive model can well characterize the deformations of metallic glass under different applied strain rates.

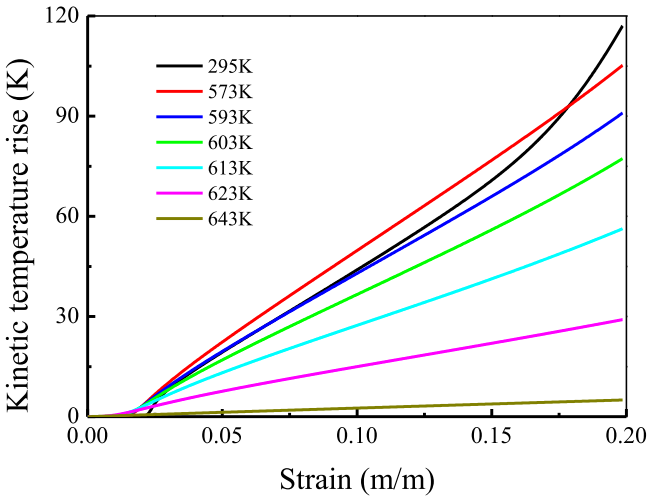

(a)

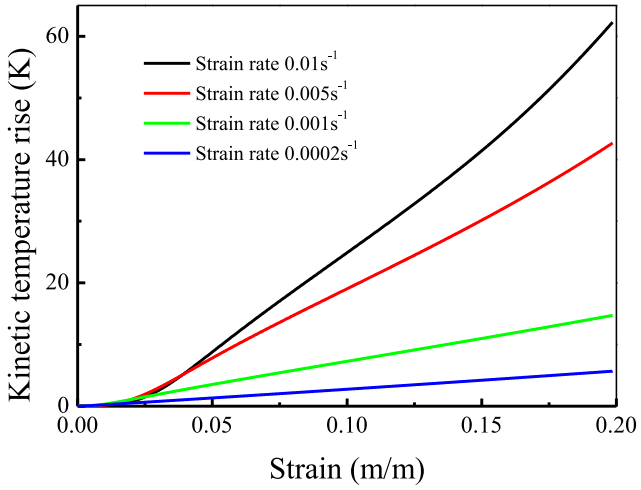

(b)

Fig. 8. The kinetic temperature-applied strain during the compressive deformation under (a) the ambient temperatures from 295K to 643K and applied strain rate of $1 \times 10^{-4}s^{-1}$, and (b) the ambient temperature of 643K and applied strain rates from $2 \times 10^{-4}s^{-1}$ to $1 \times 10^{-2}s^{-1}$.

Furthermore, two simple compression jump-in-strain-rate experiments at an ambient temperature of 643 K are also modeled. Fig. 6 (a) shows the predicted and experimental results in which the sample is first compressed at a strain rate of 0.0032 s^{-1}, and then the strain rate is instantaneously increased to 0.01 s^{-1} when the applied strain reaches 8.3%. As shown in Fig. 6(a), the predicted results are in very good agreement with the experimental results. Fig. 6(b) shows the modeling and experimental stress–strain curves in which the sample is deformed at jump-in-strain rates from 0.005 s^{-1} to 0.01 s^{-1} and back to 0.005 s^{-1} (the strains at which the jumps occur are 19.4% and 39.2%, respectively). Fig. 6(b) shows that there is a small calculation error between the predicted results and the experimental results. Thus, it can be further concluded that the strain rate dependence of deformations for metallic glass can be well described by the constructed constitutive model.

Many experiments show that the diverse modes of deformation exhibited in metallic glass are closely related to the evolution of the structure disorder degree and kinetic temperature. To investigate the origin of diverse deformation modes exhibited by metallic glass, we investigate the temporal evolution of configurational and kinetic temperatures during deformation under different ambient temperatures and applied strain rates. Fig. 7(a) gives the configurational temperatures to the response of the applied strain of the sample under different ambient temperatures (from 295 K to 643 K). It is clear that the configurational temperatures begin to increase at the onset of yielding and continue to increase rapidly until they reach equilibrium values when the ambient temperature is lower than the glass transition temperature; where the lower the ambient temperature is, the higher the equilibrium value is. However, once the ambient temperature is higher than the glass transition temperature, the configurational temperature has a slight decrease instead

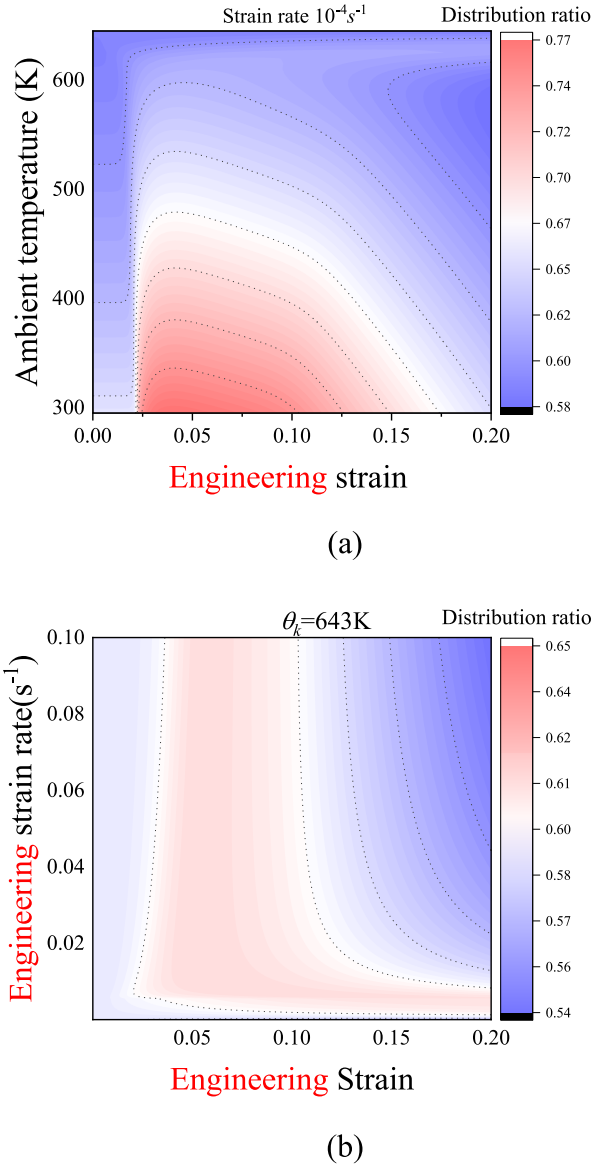

Fig. 9. The evolution of distribution ratio of dissipative energy during the deformations at different ambient temperatures and strain rates: (a) deformations at different temperatures; (b) deformations at different strain rates.

of increasing. Fig. 7(b) provides the curves of the configurational temperature and applied strain under 643 K at various strain rates from $2 \times 10^{-4}s^{-1}$ to $1 \times 10^{-2}s^{-1}$. It is determined that the strain rate and the ambient temperature have a similar effect on the evolution of configurational temperature; under a higher strain rate, the configurational temperature is more rapid to reach its equilibrium value, and the equilibrium value is larger. Fig. 8(a) and (b) show the kinetic temperature-applied strain relations under different ambient temperatures and strain rates, respectively. From Fig. 8, it can be seen that the kinetic temperatures only begin to rise if the inelastic strain is large enough (much larger than the yielding strain); with a decrease in the ambient temperature or an increase in the applied strain rate, the rise in kinetic temperature occurs much later, but the rise rate is larger. Comparing Fig. 4 with Figs. 7 and 8, it is not difficult to determine that the evolution of the configurational temperature remains at almost the same pace as the corresponding stress responses. Under different deformation modes, the configurational temperature exhibits different evolution trends. Thus, compared with the kinetic temperature, we believe that the configurational temperature has a stronger effect on the deformation of metallic glass.

As discussed in Section 2, the distribution of energy between the two subsystems is closely related to the nonequilibrium state of the total system. With an increase in nonaffine deformations, the nonequilibrium state of the total system is constantly evolving; thus, the distribution ratio of dissipative energy (i.e., $\frac{\theta_c}{\theta_c+\theta_k}$ given in Eq. (58a), (58b) is not constant. Meanwhile, the different distribution ratios have different effects on the nonequilibrium state of the total system, which plays an important role in determining the deformation

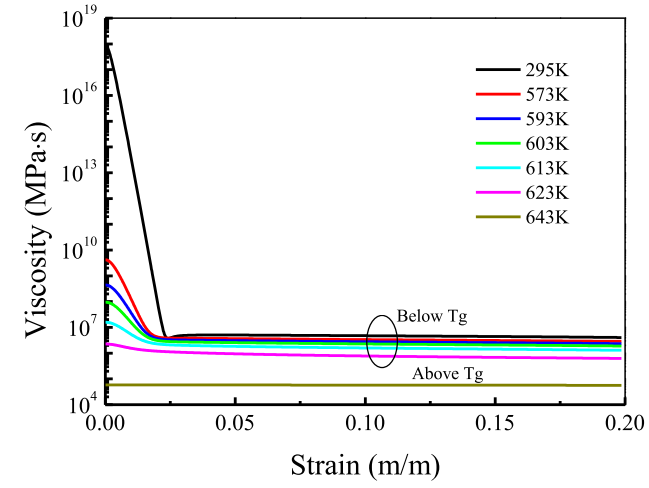

(a)

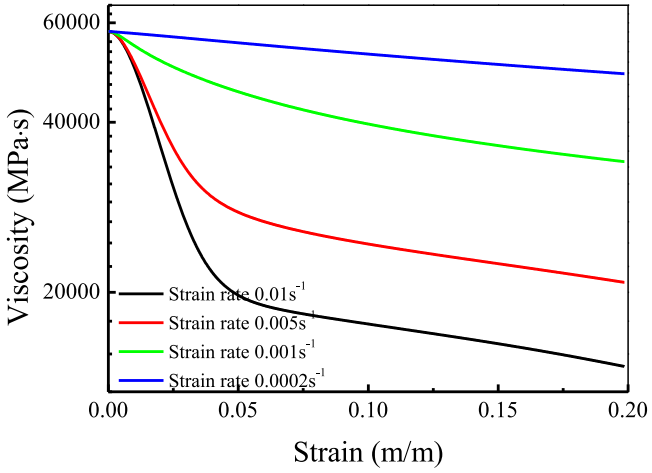

(b)

Fig. 10. The viscosity-applied strain during the compressive deformation under (a) the ambient temperatures from 295K to 643K and applied strain rate of $1 \times 10^{-4}s^{-1}$, and (b) the ambient temperature of 643K and applied strain rates from $2 \times 10^{-4}s^{-1}$ to $1 \times 10^{-2}s^{-1}$.

mode of metallic glass. In view of the distribution ratio value of energy, Fig. 9 shows the evolution of the distribution ratios of energy during the nonaffine deformation of metallic glass under different ambient temperatures and strain rates. Fig. 9(a) shows that the distribution ratio increases remarkably during deformation at room temperature when a flow stress drop occurs, while it continues to increase at a small rate during deformation at high temperatures and low strain rates. It should be noted that an obvious drop in the distribution ratios can be observed in the last stage of deformation under relatively low temperatures. Moreover, Fig. 9(a) shows that the distribution ratio of deformations at a low temperature is always larger than that of deformation at a high temperature when the ambient temperature is smaller than a critical value (a lower critical value of the glass transition temperature zone); instead, the situation often reveals the opposite when the ambient temperature is larger than such a critical value. We conclude that this difference is related to the deformation mode of metallic glass. Fig. 9(b) shows that the effect of the strain rate on the distribution ratio is slight during quasi-static deformation at high temperatures. In fact, the distribution ratio only has a slight variation with an increasing deformation and strain rate. Nevertheless, with an increase in deformation, the distribution ratio still increases first and decreases later during deformation under high temperatures. This evolution trend is similar to the trend during deformation at room temperature. As discussed in the introduction, the deformation mode of metallic glass at room temperature is different from that at high temperatures. Thus, the obvious difference between the distribution ratio of energy during deformation at room temperature and that at high temperatures can be explained.

To investigate the temperature and strain rate dependences of the microstructure evolution of metallic glass, we also investigate the

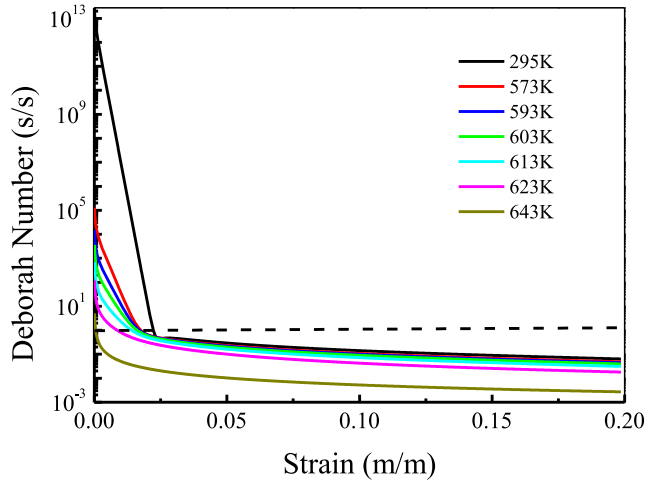

(a)

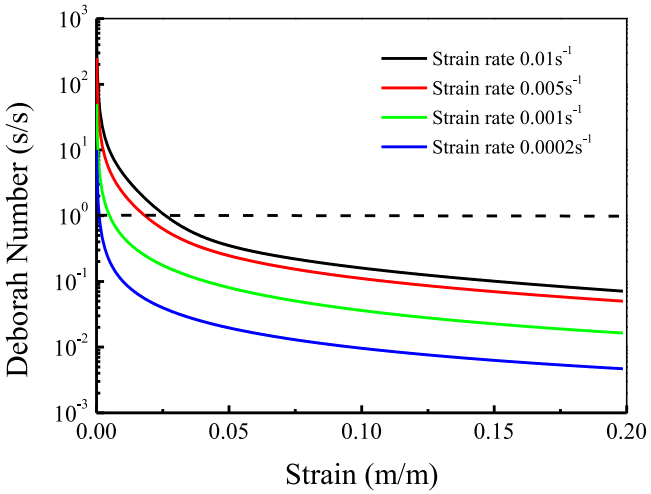

(b)

Fig. 11. The Deborah number-applied strain during the compressive deformation under (a) the ambient temperatures from 295K to 643K and an applied strain rate of $1 \times 10^{-4}s^{-1}$, and (b) the ambient temperature of 643K and applied strain rates from $2 \times 10^{-4}s^{-1}$ to $1 \times 10^{-2}s^{-1}$. (The dotted lines divided the curves into two parts whose Deborah numbers are larger than one and smaller than one, respectively).

evolution of viscosity and the Deborah number. According to the work of Jiang and Dai (2009), they can be defined as $\eta = \tau/\dot{\gamma}$ and $\kappa_c = t_r/t_e$, where $t_r = \eta/\mu$ is the Maxwell time or internal structural relaxation time under loading, and t_e is the macroscopic imposed time of external loading. Fig. 10(a) and (b) provide the viscosity-applied strain curves during deformation under different ambient temperatures and strain rates, respectively. Fig. 10(a) shows that the viscosity first drops sharply and then slightly increases before finally leveling off with a further increase in deformation when the ambient temperature is lower than the glass transition temperature. However, with an increasing ambient temperature, the initial drop in the viscosity of metallic glass becomes increasingly gentle in the early stage of deformation, and if the ambient temperature is higher than the glass transition temperature, no drop is found in the viscosity of the metallic glass. Fig. 10(b) shows that the viscosity first drops rapidly until an inflection point appears and then decreases slowly when the applied strain rate is relatively large. However, with a decrease in the applied strain rate, the declining rates of viscosity decrease in the early stage of deformation. Comparing Fig. 10 (a) with Fig. 4 and Fig. 10(b) with Fig. 5, it is determined that a significant drop in stress always occurs in the sample with an obvious drop in viscosity, and if the drop in viscosity is not obvious, then the stress drop would not occur. Fig. 11(a) and (b) show the Deborah number-applied strain relations during deformation under different ambient temperatures and different applied strain rates. From Fig. 11(a), it can be determined that the Deborah number soon decreases to be smaller than one in the early stage of deformation, and then an inflection point appears. Finally, the Deborah number continues to decrease at a small drop rate during the quasi-static deformations (the strain rate is $1 \times 10^{-4}s^{-1}$) under different

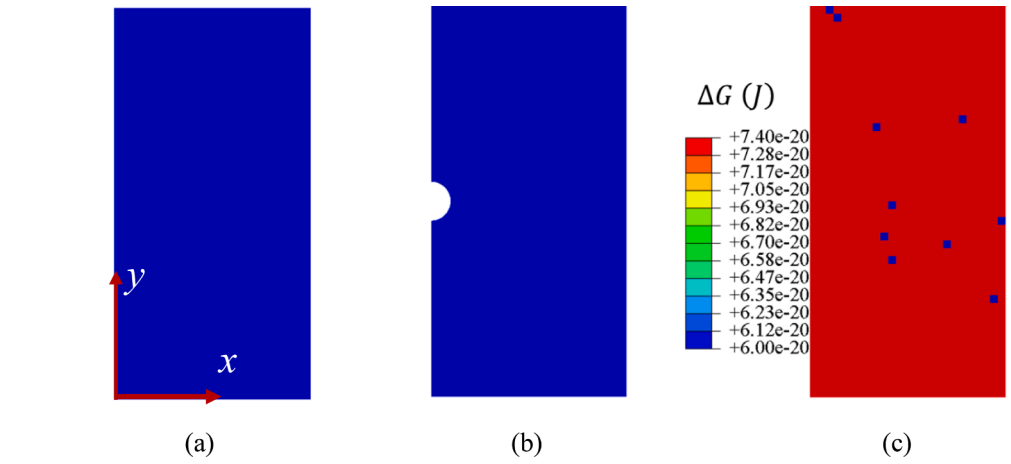

Fig. 12. The finite element model for metallic glass (a) without notch, and (b) with notch; (c) The contour for the actieval energy in the initial configuration.

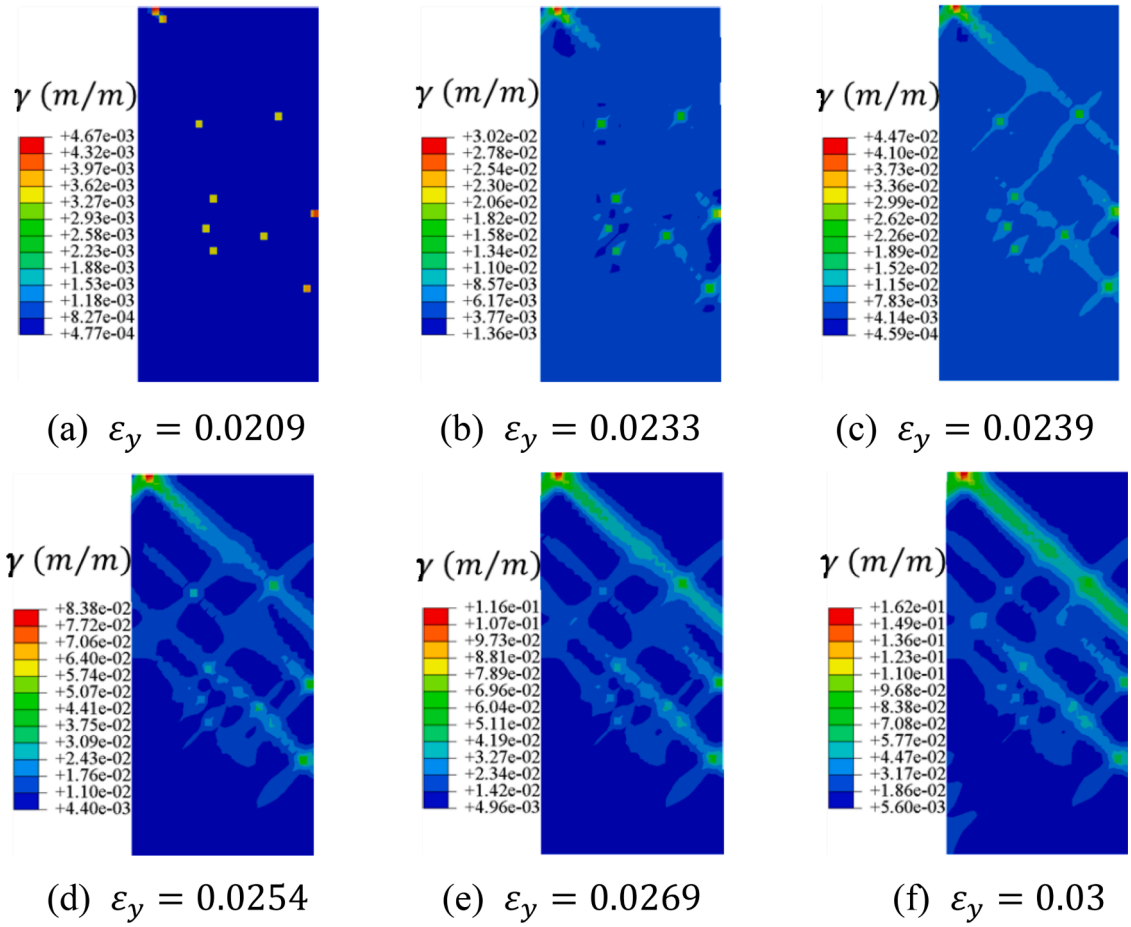

Fig. 13. The contour for the accumulated inelastic strain at different applied engineering strains.

temperatures. With an increasing ambient temperature, the Deborah numbers reach the inflection points more quickly, and the values of the Deborah number under the same applied strain are always smaller. Fig. 11(b) shows that the Deborah number first drops rapidly and then decreases slowly during deformation at 643 K and strain rates from $2 \times 10^{-4} s^{-1}$ to $1 \times 10^{-2} s^{-1}$. It should be noted that the inflection point is not obvious, and that the Deborah number may always be larger than one if the applied strain rate is sufficiently

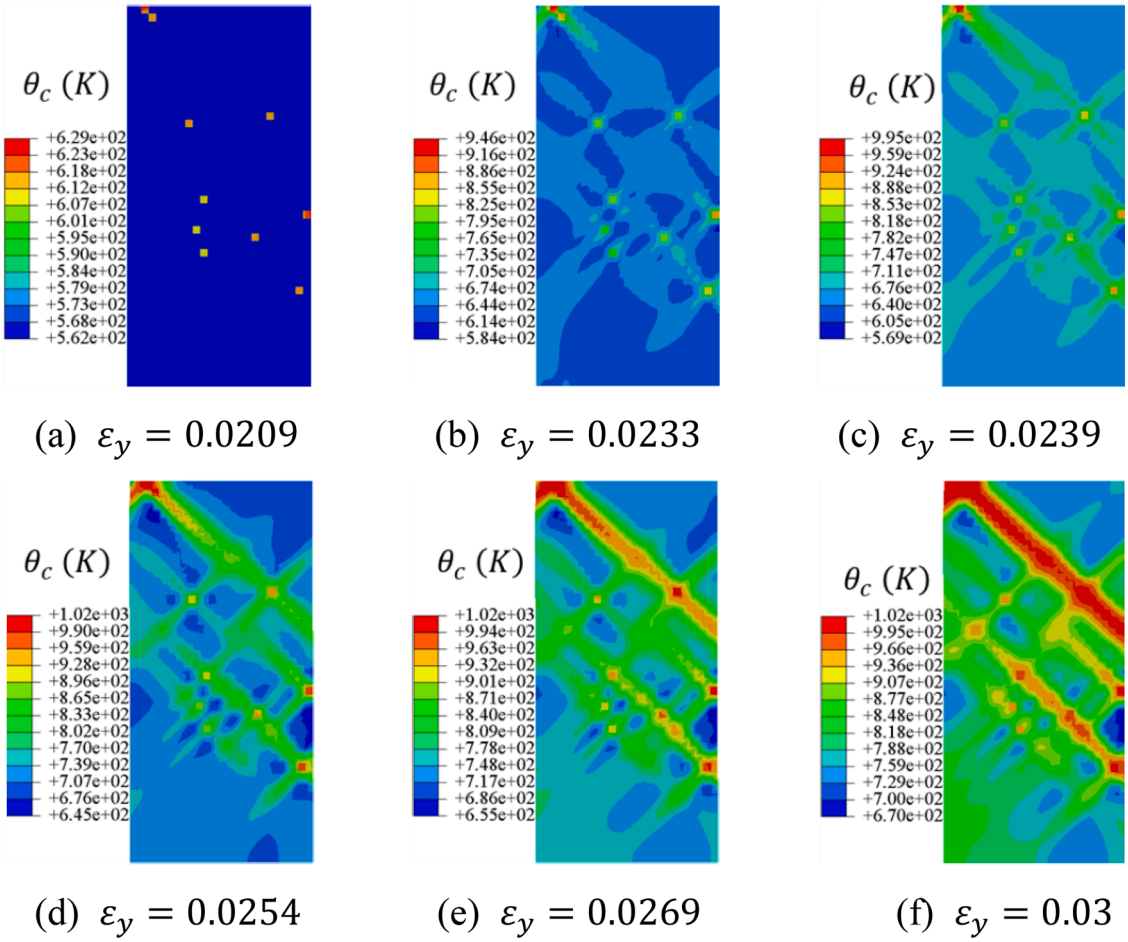

Fig. 14. The contour for the configurational temperature at different applied engineering strains.

large. From Fig. 11, we can conclude that the deformation mode of metallic glass is always transforming from the solid-like state to the liquid-like state; however, with a decrease in the ambient temperature and an increase in the applied strain rate, this transformation becomes increasingly difficult; even if the applied strain is too large or the ambient temperature is too low, this transformation may not be complete before failure occurs.

From Figs. 4, 7(a), 8(a) and 10(a), it can be determined that during the deformation of metallic glass, some shear transformations occur when the ambient temperature is smaller than the glass transition temperature, which results in a rapid drop in the viscosity. The degree of structural disorder is easier to change at lower viscosities. If the viscosity is small enough, the degree of microstructure disorder would increase rapidly with the help of the high applied stress. This rapid increase in the microstructure disorder degree would result in an increasing number of shear transformations occurring in metallic glass; subsequently, the viscosity would continue to drop rapidly, and the microstructure disorder degree would increase so rapidly that abundant shear transformations would lead to instability. A significant flow stress drop can then be observed. Finally, the microstructure disorder degrees reach their saturation points, the rate of shear transformation would also reach an equilibrium value, and the viscosity would barely change. However, with an increase in the ambient temperature, since the initial viscosity is already smaller, the drop in viscosity is slight in the early stage of deformation, although more shear transformations occur in the sample at elevated temperatures; this leads to a very low change in the degree of microstructure disorder; finally, the flow stress drop is not significant. In fact, if the ambient temperature is larger than the glass transition temperature, no flow stress drop can be found when the applied strain rate is approximately quasi-static. By comparison, we find that no obvious rise in the kinetic temperature is found until a significant flow stress drop occurs under both high and low ambient temperatures; thus, we conclude that the rise in the kinetic temperature has little effect on the flow stress drop. Remarkably, a small flow stress drop can be found when an obvious rise in the kinetic temperature occurs; however, at this stage of deformation the degree of microstructure disorder never changes. Thus, this small flow stress drop may be mainly determined by the rise in the kinetic temperature. From Fig. 11(a), with an increase in deformation the deformation mode of metallic glass always changes from a solid-like one to a liquid-like one during quasi-static deformation; however, such changes become increasingly difficult with a decrease in the ambient temperature. Under room temperature, the macroscopic response of metallic glass exhibits significant softening once some local regions complete the change of deformation mode first; subsequently, without the help of high applied

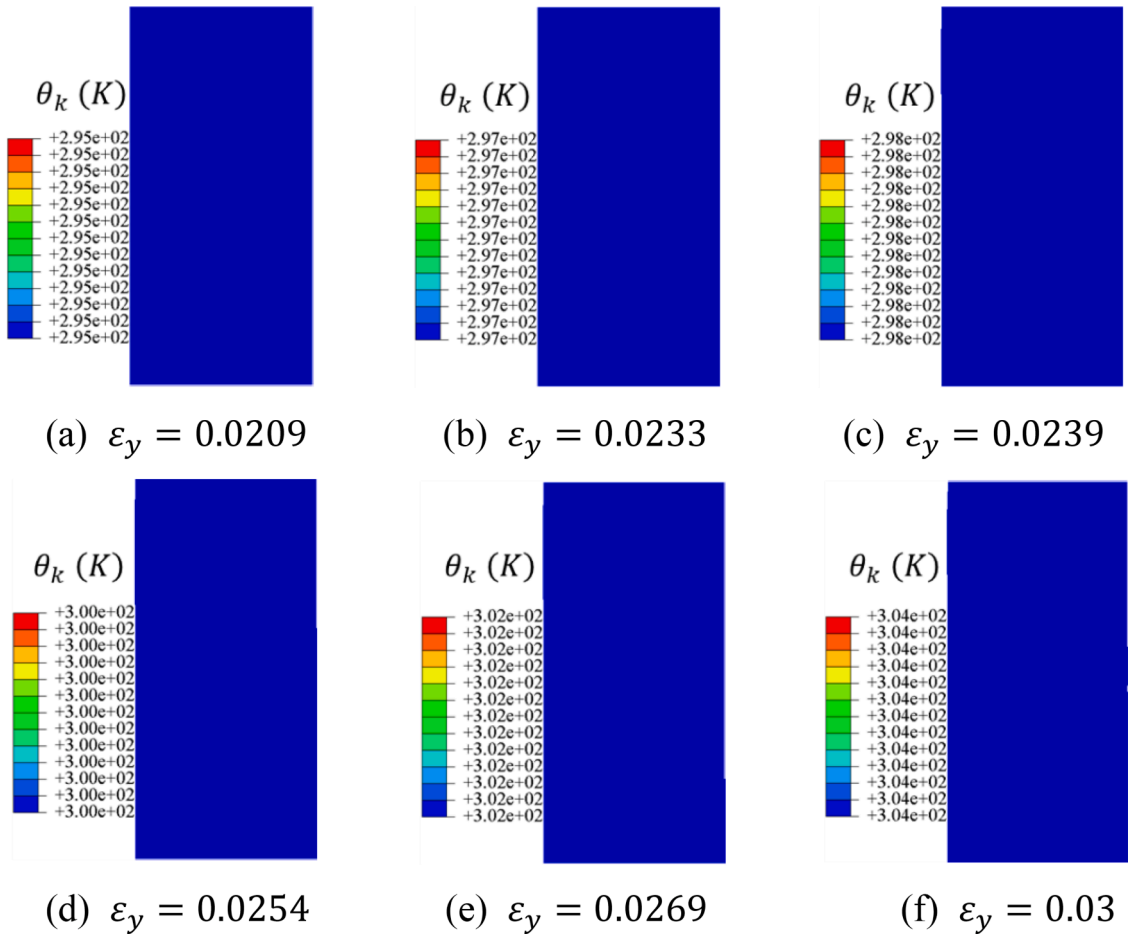

Fig. 15. The contour for the kinetic temperature at different applied engineering strains.

stress, the change in the deformation mode would not occur in the other region. However, under a high ambient temperature there is no significant flow stress drop. The change in the deformation mode in the matrix continues, even if the change in the deformation mode occurs in some local regions. Thus, the macroscopic deformation mode of metallic glass exhibits significant differences under different ambient temperatures.

Combining Figs. 5, 7(b), and 8(b) with 10(b), we find that since there is not enough time to complete a large amount of shear transformation, the yielding stress of the metallic glass rapidly increases at the early stage of deformation under a high ambient temperature (higher than the glass transition temperature) with an increasing applied strain rate; however, an increasing number of shear transformations are activated with an increasing applied loading. Thus, there is a significant drop in viscosity of the metallic glass when the strain rate is high. Such a significant drop in the viscosity makes the degree of microstructure disorder easier to change with the high applied loading; thus, with an increase in deformation, the degree of microstructure disorder increases significantly in the early stage of deformation. Subsequently, as the microstructure disorder degree increases to a critical value, avalanche-type shear transformations occur, and a relatively significant flow stress drop can be found. Finally, with the microstructure disorder degree reaching its saturation value, the flow stress generally levels off. Furthermore, Fig. 11(b) shows that with an increase in the applied strain rate, the Deborah number is more difficult down to values that are smaller than one, and its lower limit becomes larger. Thus, on the one hand shear localization may occur since there is instability during the deformation of metallic glass at a high applied strain rate; on the other hand, from the evolution tendency of the Deborah number, we find that the deformation mode changes from Newtonian flow into non-Newtonian flow since the macroscopic imposed time of external loading is so small that the internal response has insufficient time when the applied strain rate is large enough.

4.2. Shear localization

Shear localization at room temperature has seriously restricted the application of metallic glass in the engineering field. In this section, a full-field numerical simulation is conducted to investigate the evolution of the shear band in metallic glass during deformation at an ambient temperature of 295 K and a strain rate of $1 \times 10^{-4} s^{-1}$. As is known, a shear band is a form of plastic instability

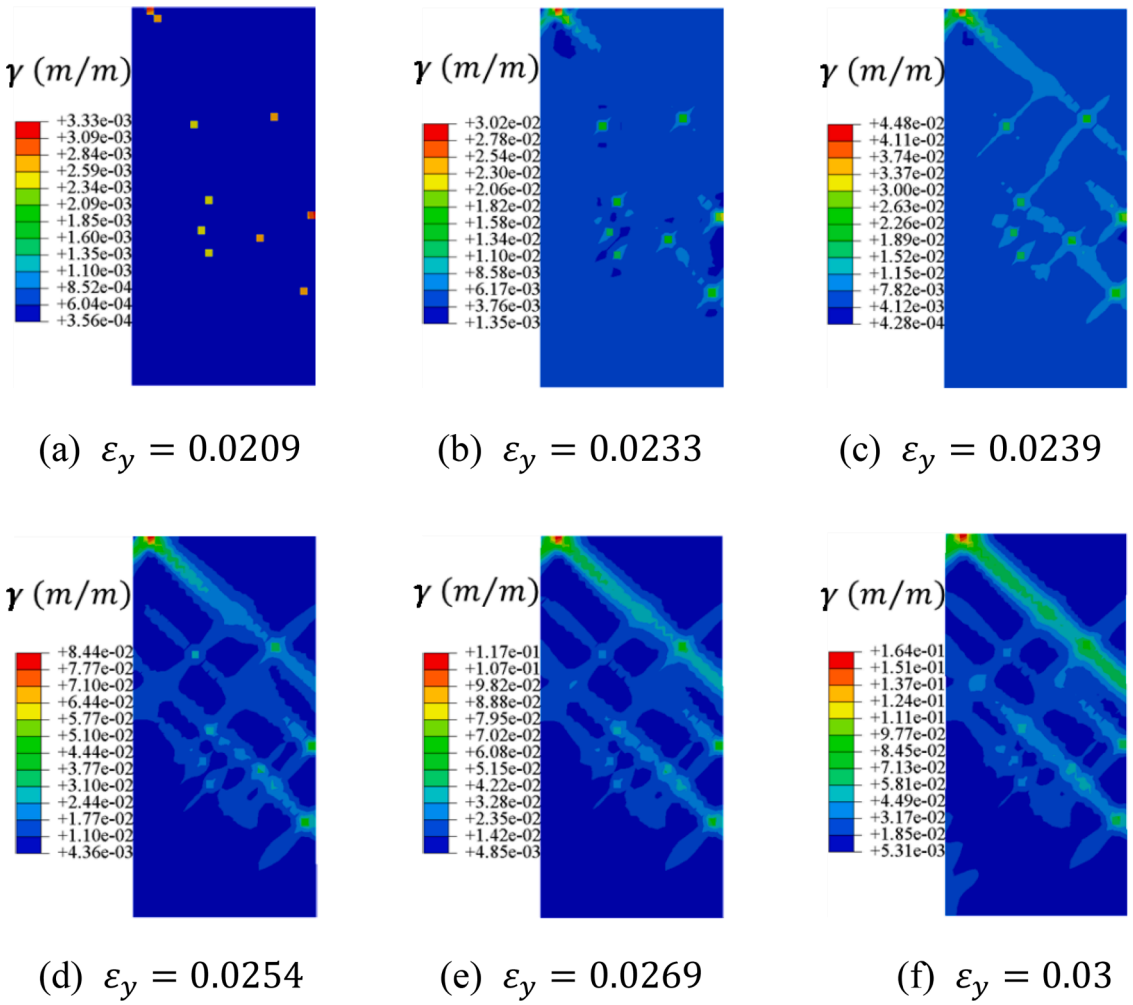

Fig. 16. The contour for the accumulated inelastic strain at different applied engineering strains predicted by the constitutive model with neglecting the diffusion term of configurational temperature.

that localizes large shear strains in a relatively thin band when a material is deformed. Thus, we use the distribution nephogram of accumulative inelastic strain to characterize the evolution of the shear band in this work.

To effectively capture the main evolution characteristics of the microstructure, we should build a suitable finite element model. To be more convenient towards directly observing the evolution of shear bands without losing generality, a 2-D axial plane strain finite element model is used in this work according to the work of Rao et al. (2018). Fig. 12 (a) and (b) show the finite element model of the metallic glass without and with a notch, respectively. The sizes for these two samples in the numerical simulation are 0.5 μm in width and 1 μm in height. In Fig. 12(b), the radius of the semicircular notch is 0.1 μm. To reasonably consider the thermomechanical coupling of metallic glass, the CPE4R element is adopted to mesh the finite element model. To capture the main characteristics of the shear band, the size of the mesh in Fig. 12(a) is set as approximately 20 nm, which matches the characteristic dimension of the shear band; to capture the characteristic of microstructure evolution at the notch root as effectively as possible, we set the size of the mesh in Fig. 12 (b) as approximately 10 nm. Furthermore, to effectively describe the local deformation in the sample without a notch, we introduce some initial defects into the sample, as shown in Fig. 12(c), by referring to the work of Rao et al. (2018) and Thamburaja (2011).

The experiment shows that the shear localization is very significant during both the tensile and compressive deformations (Greer et al., 2013). Here, the evolution of shear band during tensile deformation is investigated. In fact, since the effect of pressure has been neglected, the following predicted conclusions are also suitable for the compressive deformation. To model the deformation of the metallic glass during the monotonic uniaxial tensile loading along the y-direction shown in Fig. 11, the displacement boundary conditions are applied as follows for the domain ($0<x<l_1$, $0<y<l_2$): $u_x(0,0) = u_y(0,0) = 0$; $u_y(x,0) = 0$; $u_y(x,l_2) = \delta$; and δ is the applied displacement. All simulations in this section are conducted using a strain-controlled numerical algorithm at a constant strain rate of $1 \times 10^{-4}\ s^{-2}$ and an ambient temperature of 295 K. During the deformation of the test specimens conducted by Lu (2002), a thermocouple placed next to the surface of the specimens were measuring fluctuations of 0.5 K (relative to ambient temperature). Here, we will fix the kinetic temperature on the remaining four outer surfaces of the finite-element mesh to remain at the respective

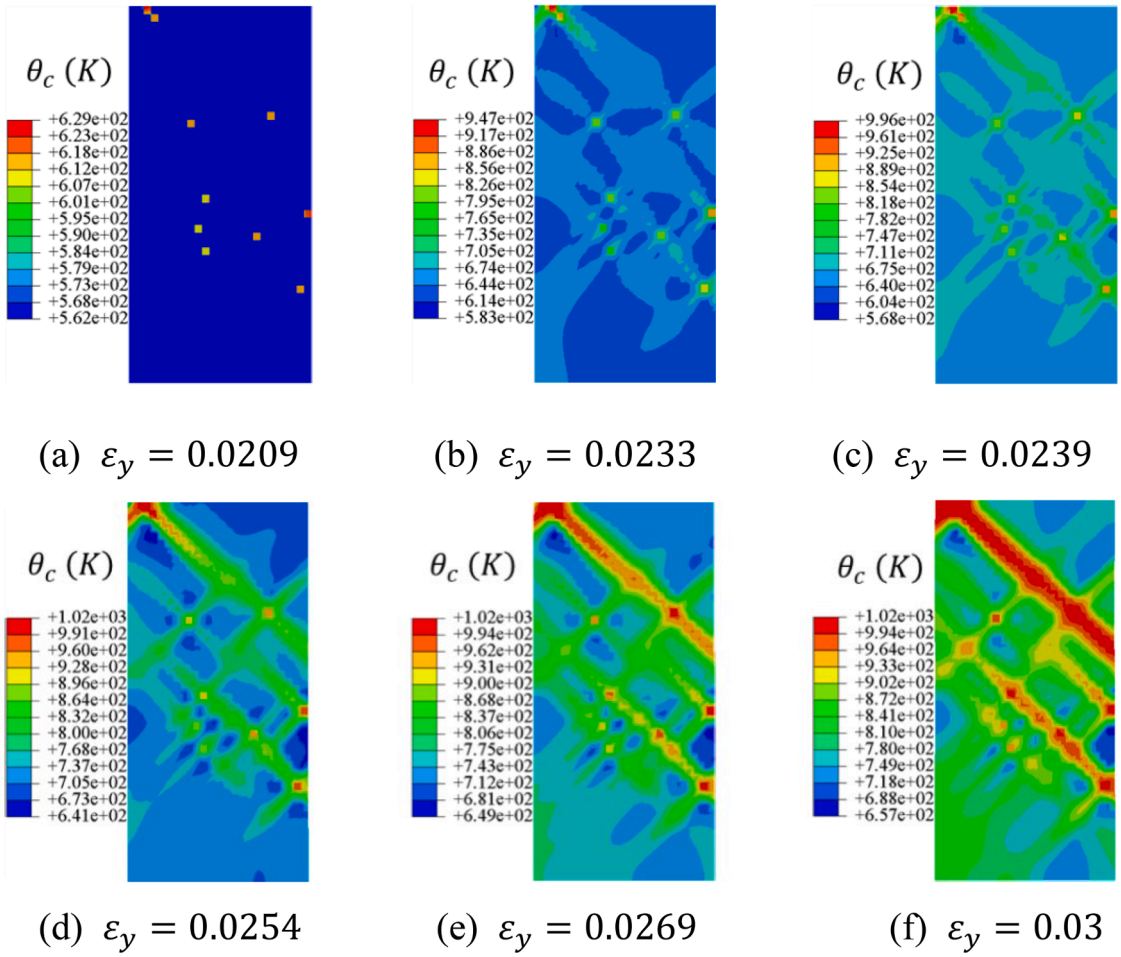

Fig. 17. The contour for the configurational temperature at different applied engineering strains with neglecting the diffusion term of configurational temperature.

ambient temperature. Since the configuration temperature is only used to characterize the nonequilibrium phenomena in amorphous materials, there could exist no energy exchange between configuration subsystem and surrounding environment directly. Then, the adiabatic boundary condition is set for configuration subsystem.

Figs. 13–15 show the contours of accumulative inelastic strain and configurational and kinetic temperatures in metallic glass without a notch, respectively. The formation of shear band can be divided into three consecutive stages. First, in the early stage of deformation, since the activation energy in the defect regions is smaller than that in the matrix, shear localization first occurs in these defect regions. Second, several viable bands for shearing are created with the help of the local stress concentration. In these bands the viscosity begins to decrease rapidly; thus, the evolution of the microstructure becomes easier. Then the structure inside is disordered in these bands with the help of applied loading. Due to structural rejuvenation, the activation rate of shear transformation along these bands becomes increasingly larger. However, it should be noted that the inelastic strain throughout the band is not large in this stage, and that the local heating resulting from the plastic dissipation can be neglected. Finally, following the creation of the softened path, an increasing amount of shear transformation occurs in these bands, and inelastic instability is pioneered in one of these bands. Then, the large plastic strains rapidly undergo inelastic instability in the band. As a result, a main shear band with significant shear localization is created. In the third stage, the shear-band material experiences such large plastic strains that significant heating is now possible; however, since the thermal diffusivity is quite high, this local heating disperses so rapidly that the kinetic temperature field in the entire sample is homogeneous. Thus, the increase in kinetic temperature is very small in the stage of shear band formation. This predicted formation process of the shear band is similar to that discussed in the two-stage scenario (Greer et al., 2013). However, it should be noted that these three stages are not independent of one another in the time domain; in fact, the next stage has begun before the previous step completes.

To reveal the effect of the nonlocal diffuse term of the configurational temperature on the evolution of shear band, we also adopt the constitutive model neglecting the diffusion term of the configurational temperature to model the tensile deformation of metallic glass at room temperature (295 K) and a quasi-static strain rate of $1 \times 10^{-4}\ s^{-2}$. Figs. 16 and 17 show the predicted distribution of the accumulative inelastic strain and configurational temperature, respectively. Comparing Fig. 13 with Fig. 16, it can be determined that

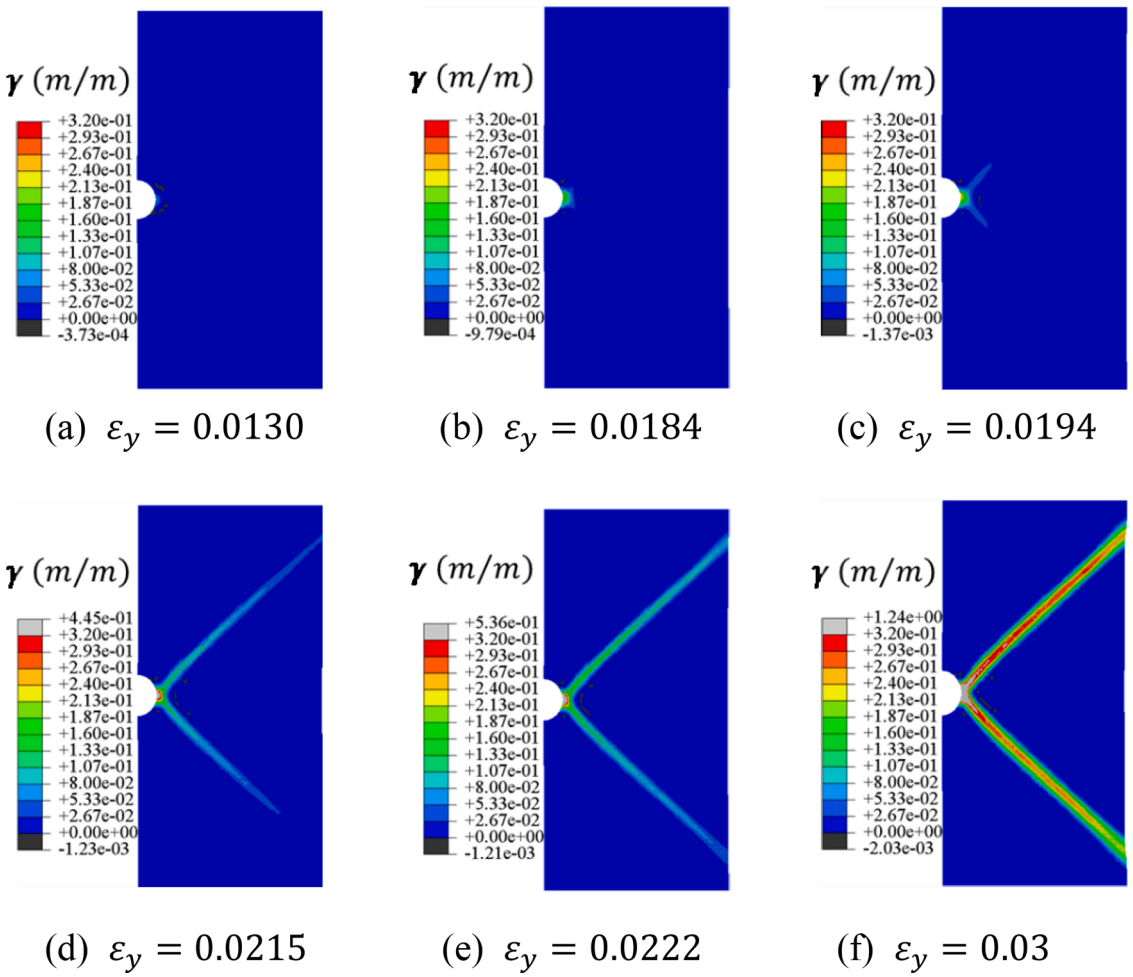

Fig. 18. The contour for the accumulated inelastic strain at different applied engineering strains in the sample with notch.

the nonlocal term in the configurational relation has little effect on the evolution of the shear band. Comparing Fig. 14 with Fig. 17, we also find that there is little difference between these two predicted distributions of the configurational temperature. These results imply that for large-volume samples (where the size of the sample is larger than 0.5 μm), the nonlocal term in the configurational relations has a negligible effect on the overall deformation behavior of the sample. This conclusion agrees with the results in the work of Thamburaja (2011).

Figs. 18 and 19 show the modeling contours of the accumulative inelastic strain and configurational temperature of the metallic glass sample with a notch, respectively. Remarkably, since the nonlocal term in the configurational relations has little effect on the deformation of the large-volume sample, the diffusion term of the configurational temperature is also neglected in this simulation, so that a large amount of computer cost can be saved. Figs. 18 and 19 show that many shear transformations first occur at the notch root with the help of a high local stress, and then an obvious local inelastic zone forms. With an increasing deformation, on the one hand the size of such an inelastic zone increases; on the other hand, the localization degree is more significant. Once the size of the inelastic zone is larger than a critical value, the viable bands for shearing begin to be launched from the notch root to the other side of the sample. In these viable bands, the configurational temperature reached a critical value, which did not increase with an increasing deformation. Then, following the formation of viable bands, significant plastic deformation occurs in this viable band, and the realistic shear band passes through the sample rapidly. This indicates that the precondition of shear band propagation is that the disorder degree of the microstructure in the local zone needs to reach a saturation value. Furthermore, it is also determined that the viable bands become wider when significant shear localization occurs in such viable bands. This indicates that there is an apparent competition between the sharp shear localization and diffuse shear during the tensile deformation of a sample with a notch. If the diffuse shear banding is significant, then necking of the ligament may be found under tension; otherwise, catastrophic failure will take place.

5. Conclusions

Based on the out-of-equilibrium statistical concept and the STZ concept, a finite deformation constitutive model was developed

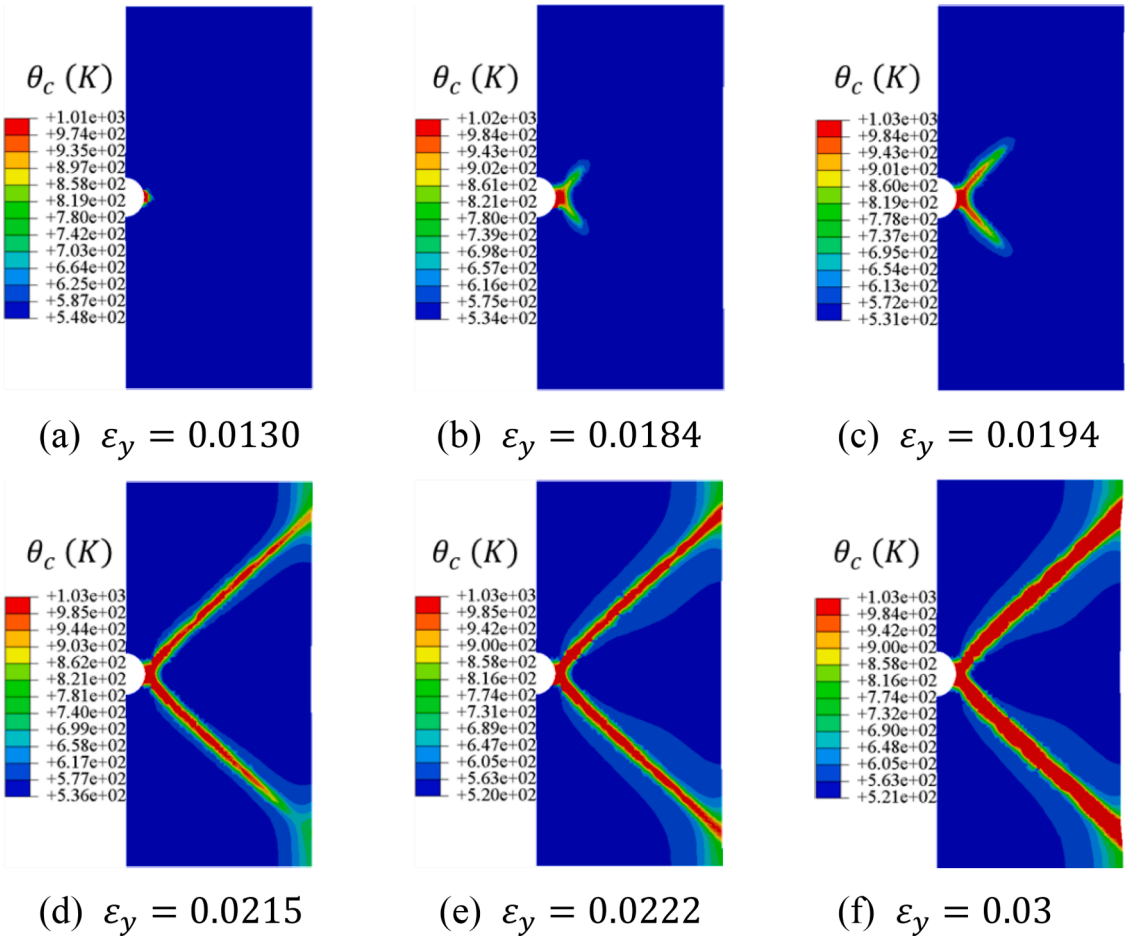

Fig. 19. The contour for the configurational temperature at different applied engineering strains in the sample with notch.

within the thermodynamic framework of an irreversible continuum medium. In this constitutive model, metallic glass is regarded as a solid composed of weakly interacting configurational and kinetic subsystems, so that the mismatching of time scales between the vibrations around a mechanically stable microscopic configuration and structural evolution can be reasonably dealt with. Moreover, a locally stored transformation energy was introduced into the evolution equation of inelastic shear strain to consider the reverse shear transformation, which is caused by a strain energy field accumulated along with the shear transformation. To verify the effectiveness of the newly developed constitutive model in predicting the deformation of metallic glass, this constitutive model was implemented into a finite element code by writing a UMAT; then, the deformations of metallic glass under different loading conditions were modeled. The predicted results were compared with the corresponding experiments and theories, and three important conclusions were obtained as follows:

(1) The main deformation mechanisms of metallic glass are well captured by the newly constructed constitutive model, and then the deformation of metallic glass under different ambient temperatures and applied strain strains can be effectively predicted.
(2) The developed model shows that the deformation modes exhibited by metallic glass are related to the configuration disorder degree, which determines the internal structural relaxation time. The internal structural relaxation time is large, and metallic glass exhibits a solid-like behavior if the configuration disorder degree is relatively small; otherwise, metallic glass exhibits liquid-like behavior.
(3) Based on the new model, it is determined that the precondition of shear band formation is that the viable band, in which the configuration disorder degree reaches a saturation value, is created for shear.

Declaration of Competing Interest

None.

Acknowledgement

This work is financially supported by the NSFC (Nos. 11790292, 12002342, 11972346 and No. 11672299), the NSFC Basic Science Center Program for "Multiscale Problems in Nonlinear Mechanics" (No.11988102), the Strategic Priority Research Program (No. XDB22040302 and No. XDB22040303), the Key Research Program of Frontier Sciences (Grant No. QYZDJSSW-JSC011), the opening project of State Key Laboratory of Explosion Science and Technology (Beijing Institute of Technology, No. KFJJ18-14M).

Reference

Anand, L., Gurtin, M.E., 2003. A theory of amorphous solids undergoing large deformations, with application to polymeric glasses. Int. J. Solids Struct. 40, 1465–1487.
Anand, L., Su, C., 2005. A theory for amorphous viscoplastic materials undergoing finite deformations, with application to metallic glasses. J. Mech. Phys. Solids 53, 1362–1396.
Anand, S., Su, C., 2007. A constitutive theory for metallic glasses at high homologous temperatures. Acta Mater. 55, 3735–3747.
Argon, A.S., 1979. Plastic deformation in metallic glasses. Acta Metall. 271, 47–58.
Bargmann, S., Xiao, T., Klusemann, B., 2014. Computational modelling of submicron-sized metallic glasses. Philos. Mag. 94, 1–19.
Bouchbinder, E., Langer, J.S., 2009. Nonequilibrium thermodynamics of driven amorphous materials. II. effective-temperature theory. Phys. Rev. E 80, 031132-1-094505-7.
Bouchbinder, E., Langer, J.S., Procaccia, I., 2007. Athermal shear-transformation-zone theory of amorphous plastic deformation. II. Analysis of simulated amorphous silicon. Phys. Rev. E 80, 031132.
Cheng, Y.T., Hao, Q., Pelletier, J.M., et al., 2021. Modelling and physical analysis of the high-temperature rheological behavior of a metallic glass. Int. J. Plast. 146, 103107.
Cohen, M.H., Turnbull, D., 1959. Molecular transport in liquids and glasses. J. Chem. Phys. 31, 1164–1169.
Cugliandolo, L.F., 2011. The effective temperature. J. Phys. A Math. Theor. 44 (48), 483001.
Dai, L.H., Bai, Y.L., 2007. Basic mechanical behaviors and mechanics of shear banding in BMGs. Int. J. Impact Eng. 35, 704–716.
Dutta, T., Chauniyal, A., Singh, I., et al., 2018. Plastic deformation and failure mechanisms in nano-scale notched metallic glass specimens under tensile loading. J. Mech. Phys. Solids 111, 393–413.
Dutta, T., Narasimhan, R., 2020. Numerical study of stationary cracks in bulk metallic glass composites under Mode I, small scale yielding conditions. Eng. Fract. Mech. 239, 107312.
Falk, M.L., Langer, J.S., 1998. Dynamics of viscoplastic deformation in amorphous solids. Phys. Rev. E 57 (6), 7192–7205.
Falk, M.L., Langer, J.S., 2011. Deformation and failure of amorphous, solidlike materials. Annu. Rev. Condens. Matter Phys. 2, 353–373.
Gan, K.F., Jiang, S.S., Huang, Y.J., et al., 2019. Elucidating how correlated operation of shear transformation zones leads to shear localization and fracture in metallic glasses: tensile tests on CuZr based metallic-glass microwires, molecular dynamics simulations, and modelling. Int. J. Plast. 119, 1–20.
Gao, Y.F., Wang, L., Bei, H., et al., 2011. On the shear-band direction in metallic glasses. Acta Mater. 59 (10), 4159–4167.
Greer, A.L., Cheng, Y.Q., Ma, E., 2013. Shear bands in metallic glasses. Mater. Sci. Eng. R 74, 71–132.
Han, D., Wei, D., Cao, P., et al., 2020. Statistical complexity of potential energy landscape as a dynamic signature of the glass transition. Phys. Rev. B 101, 64205.
Hasan, O.A., Boyce, M.C., 2010. A constitutive model for the nonlinear viscoelastic viscoplastic behavior of glassy polymers. Polym. Eng. Sci. 35, 331–344.
Henann, D.L., Anand, L., 2008. A constitutive theory for the mechanical response of amorphous metals at high temperatures spanning the glass transition temperature: Application to microscale thermoplastic forming. Acta Mater. 56, 3290–3305.
Homer, E.R., Li,, L., Schuh, C.A., 2016. Kinetic Monte Carlo Modeling of Nanomechanics in Amorphous Systems. Springer, pp. 441–468.
Homer, E.R., Rodney, D., Schuh, C.A., 2010. Kinetic Monte Carlo study of activated states and correlated shear-transformation-zone activity during the deformation of an amorphous metal. Phys. Rev. B 81 (6), 064204.
Huang, R., Suo, Z., Prevost, J.H., et al., 2002. Inhomogeneous deformation in metallic glasses. J. Mech. Phys. Solids 50, 1011–1027.
Hufnagel, T.C., Schuh, C.A., Falk, M.L., et al., 2016. Deformation of metallic glasses: recent developments in theory, simulations, and experiments. Acta Mater. 109, 375–393.
Jia, H., Wang, G., Chen, S., et al., 2018. Fatigue and fracture behavior of bulk metallic glasses and their composites. Prog. Mater Sci. 98, 168–248.
Jiang, M.Q., Dai, L.H., 2009. On the origin of shear banding instability in metallic glasses. J. Mech. Phys. Solids 57 (8), 1267–1292.
Jiang, S., Huang, Y., Xue, P., et al., 2021. Temperature-dependent deformation behavior of a CuZr-based bulk metallic glass composite. J. Alloys Compd. 858, 158368.
Jiang, S.S., Gan, K.F., Huang, Y.J., et al., 2020. Stochastic deformation and shear transformation zones of the glassy matrix in CuZr-based metallic-glass composites. Int. J. Plast. 125, 52–62.
Kamrin, K., Bouchbinder, E., 2014. Two-temperature continuum thermomechanics of deforming amorphous solids. J. Mech. Phys. Solids 73, 269–288.
Karmakar, S., Dasgupta, C., Sastry, S., Langer, J.S., 2014. Growing length scales and their relation to timescales in glass-forming liquids. Annu. Rev. Condens. Matter Phys. 5, 255–284.
Kawamura, Y., Nakamura, T., Inoue, A., 1998. Superplasticity in $Pd_{40}Ni_{40}P_{20}$ metallic glass. Scr. Mater. 39 (3), 301.
Kondori, B., Benzerga, A.A., Needleman, A., 2016. Discrete shear transformation zone plasticity. Extrem. Mech. Lett. 9, 21–29.
Kondori, B., Benzerga, A.A., Needleman, A., 2018. Discrete shear-transformation-zone plasticity modeling of notched bars. J. Mech. Phys. Solids 111, 18–42.
Kosiba, K., Şopu, D., Scudino, S., et al., 2019. Modulating heterogeneity and plasticity in bulk metallic glasses: role of interfaces on shear banding. Int. J. Plast. 119, 156–170.
Lin, W.H., Teng, Y., Sha, Z.D., et al., 2020. Mechanical properties of nanoporous metallic glasses: insights from large-scale atomic simulations. Int. J. Plast. 127, 102657.
Liu, C., Yan, X., Sharma, P., et al., 2020. Unraveling the non-monotonic ageing of metallic glasses in the metastability-temperature space. Comput. Mater. Sci. 172, 109347.
Lu, J., 2002. Mechanical Behavior of a Bulk Metallic Glass and its Composite Over a Wide Range of Strain Rates and Temperatures. California Institute of Technology.
Manning, M.L., Daub, E.G., Langer, J.S., et al., 2009. Rate-dependent shear bands in a shear-transformation-zone model of amorphous solids. Phys. Rev. E 79, 016110.
Nicolas, A., Ferrero, E.E., Martens, k., et al., 2018. Deformation and flow of amorphous solids: Insights from elastoplastic models. Rev. Mod. Phys. 90, 045006.
Qu, S., 2004. A conventional theory of mechanism-based strain gradient plasticity. Urbana, Illinois.
Rao, W., Zhang, J., Kang, G.Z., 2018. A failure mechanism based constitutive model for bulk metallic glass. Mech. Mater. 125, 52–69.
Rao, W., Zhang, J., Kang, G., et al., 2019. A meso-mechanical constitutive model of bulk metallic glass composites considering the local failure of matrix. Int. J. Plast. 115, 238–267.
Rodney, D., Schuh, C.A., 2009. Yield stress in metallic glasses: the jamming-unjamming transition studied through Monte Carlo simulations based on the activation-relaxation technique. Phys. Rev. B 80 (18).
Rodney, D., Tanguy, A., Vandembroucq, D., 2011. Modeling the mechanics of amorphous solids at different length scale and time scale. Modell. Simul. Mater. Sci. Eng. 19 (8), 083001.
Schuh, C.A., Hufnagel, T.C., Ramamurty, U., 2007. Mechanical behavior of amorphous alloys. Acta Mater. 55, 4067–4109.
Sha, Z.D., Lin, W.H., Poh, L.H., et al., 2020. Fatigue of metallic glasses. Appl. Mech. Rev. 72 (5), 050801.
Shi, Y.F., Katz, M., Li, H., Falk, M.L., 2007. Evaluation of the disorder temperature and free-volume formalisms via simulations of shear banding in amorphous solids. Phys. Rev. Lett. 98 (18), 185505.

Singh, I., Guo, T.F., Murali, P., et al., 2013. Cavitation in materials with distributed weak zones: implications on the origin of brittle fracture in metallic glasses. J. Mech. Phys. Solids 61 (4), 1047–1064.
Singh, I., Guo, T.F., Narasimhan, R., et al., 2014. Cavitation in brittle metallic glasses - effects of stress state and distributed weak zones. Int. J. Solids Struct. 51, 4373–4385.
Sollich, P., Cates, M.E., 2012. Thermodynamic interpretation of soft glassy rheology models. Phys. Rev. E 85, 031127.
Spaepen, F., 1977. A microscopic mechanism for steady state inhomogeneous flow in metallic glasses. Acta Metall. 25, 407–415.
Srivastava, V., Chester, S.A., Ames, N.M., et al., 2010. A thermo-mechanically-coupled large-deformation theory for amorphous polymers in a temperature range which spans their glass transition. Int. J. Plast. 26, 1138–1182.
Sun, B.A., Wang, W.H., 2015. The fracture of bulk metallic glasses. Prog. Mater Sci. 74, 211–307.
Takeuchi, S., Edagawa, K., 2011. Atomistic simulation and modeling of localized shear deformation in metallic glasses. Prog. Mater Sci. 56, 785–816.
Tandaiya, P., Ramamurty, U., Ravichandran, G., et al., 2008. Effect of Poisson's ratio on crack tip fields and fracture behavior of metallic glasses. Acta Mater. 56, 6077–6086.
Tandaiya, P., Ramamurty, U., Narasimha, R., 2009. Mixed mode (I and II) crack tip fields in bulk metallic glasses. J. Mech. Phys. Solids 57, 1880–1897.
Tandaiya, P., Narasimha, R., Ramamurty, U., 2009. On the mechanism and the length scales involved in the ductilefracture of a bulk metallic glass. Acta Mater. 61 (5), 1558–1570.
Tang, X.C., Yao, X.H., Wilkerson, J.W., 2021. A micromechanics-based framework to predict transitions between dimple and cup-cone fracture modes in shocked metallic glasses. Int. J. Plast. 137, 102884.
Thamburaja, P., 2011. Length scale effects on the shear localization process in metallic glasses: a theoretical and computational study. J. Mech. Phys. Solids 59, 1552–1575.
Thamburaja, P., Ekambaram, R., 2007. Coupled thermo-mechanical modelling of bulk-metallic glasses: theory, finite-element simulations and experimental verification. J. Mech. Phys. Solids 55, 1236–1273.
Thamburaja, P., Liu, J., 2014. Effects of microscopic boundary conditions on the deformation behaviorof small-volume metallic glasses. Int. J. Solids Struct. 51, 4580–4595.
Turnbull, D., Cohen, M.H., 1970. On the free-volume model of the liquid-glass transition. J. Chem. Phys. 52, 3038.
Van, Loock, F., Brassart, L., Pardoen, T., 2021. Implementation and calibration of a mesoscale model for amorphous plasticity based on shear transformation dynamics. Int. J. Plast. 145, 103079.
Vasoya, M., Kondori, B., Benzerga, A.A., et al., 2020. Energy dissipation rate and kinetic relations for Eshelby transformations. J. Mech. Phys. Solids 136, 103699.
Wang, W.H., 2012. The elastic properties, elastic models and elastic perspectives of metallic glasses. Prog. Mater Sci. 57, 487–656.
Wang, Z., Sun, B.A., Bai, H.Y., et al., 2014. Evolution of hidden localized flow during glass-to-liquid transition in metallic glass. Nat. Commun. 5 (1), 5823. -5823.
Xiao, R., Choi, J., Lakhera, N., et al., 2013. Modeling the glass transition of amorphous networks for shape-memory behavior. J. Mech. Phys. Solids 61 (7), 1612–1635.
Xiao, R., Nguyen, T.D., 2015. An effective temperature theory for the nonequilibrium behavior of amorphous polymers. J. Mech. Phys. Solids 82, 62–81.
Xie, X., Lo, Y.C., Tong, Y., et al., 2019. Origin of serrated flow in bulk metallic glasses. J. Mech. Phys. Solids 124, 634–642.
Xue, S.L., Li, B., Feng, X.Q., et al., 2017. A non-equilibrium thermodynamic model for tumor extracellular matrix with enzymatic degradation. J. Mech. Phys. Solids 104, 32–56.
Yang, Q., Mota, A., Ortiz, M., 2006. A finite-deformation constitutive model of bulk metallic glass plasticity. Comput. Mech. 37, 194–204.
Yuan, S., Branicio, P.S., 2020. Gradient microstructure induced shear band constraint, delocalization, and delayed failure in CuZr nanoglasses. Int. J. Plast. 134, 102845.
Zhang, Z., Wang, C., Liu, P., et al., 2022. Deformation behavior of a nanoporous metallic glass at room temperature. Int. J. Plast., 103232
Zhu, W.Q., Liu, J.J., Wei, X.D., 2021. A new continuum model for viscoplasticity in metallic glasses based on thermodynamics and its application to creep tests. J. Mech. Phys. Solids 146, 104216.